TECHNICAL MEMORANDUMS

NATIONAL ADVISORY COMMITTEE FOR AERONAUTICS

No. 946

EXPERIMENTAL RESULTS WITH AIRFOILS TESTED IN THE HIGH-SPEED TUNNEL AT GUIDONIA

By Antonio Ferri

Atti di Guidonia
No. 17, September 20, 1939

Washington
July 1940

NATIONAL ADVISORY COMMITTEE FOR AERONAUTICS

TECHNICAL MEMORANDUM NO. 946

EXPERIMENTAL RESULTS WITH AIRFOILS TESTED IN THE HIGH-SPEED TUNNEL AT GUIDONIA*

By Antonio Ferri

SUMMARY

The results are presented of a triple series of tests using force measurements, pressure-distribution measurements, and air-flow photographs, on airfoil sections suitably selected so that comparison could be made between the experimental and theoretical results. The comparison with existing theory is followed by a discussion of the divergences found and an attempt is made to find their explanation.

INTRODUCTION

The first series of high-speed tests conducted at Guidonia was undertaken with the object of checking experimentally the aerodynamic theories for the field of supersonic velocities - these theories as yet not confirmed or supported by experiment. The airfoils tested were so chosen that their characteristics could be computed theoretically by relatively simple computations and thus be compared with the results obtained experimentally. For this purpose the airfoil sections selected were bounded by either straight lines or circular arcs and were of sufficient thickness to permit the required strength and resistance to flexural deformation. Air-force measurements were conducted on all the wing sections - four in number - while pressure-distribution measurements and optical investigations were conducted on two of them. Since the force measurements yielded results that deviated to some extent from those predicted by the theory, the pressure-distribution measurements were found very useful as they clearly showed up the divergences from the theory, while the optical observations, by confirming the pressure measurements, led to some hypotheses as to the reason for these divergences.

*"Alcuni Risultati Sperimentali Riguardanti Profili Alari Provati alla Galleria Ultrasosonora di Guidonia." Atti di Guidonia, No. 17, September 20, 1939.

EXPERIMENTAL METHODS

The tests were all conducted at two Mach numbers, namely, 1.85 and 2.13. The tunnels in which such high speeds could be obtained were of the usual type, that is, with a diffuser gradually diverging from the throat section up to the test chamber. Such passages were obtained after numerous attempts to eliminate the shock waves formed in the neighborhood of the throat; but whereas the elimination was complete in one of them, the shocks still remained in the other near the critical section. Since, however, the optical observations and the pressure measurements showed that the disturbances created by these shocks were negligible and that the subsequent expansion in the diffuser occurred regularly, tests were also conducted in this tunnel.

The velocity was obtained by pressure measurements upstream and downstream of the tunnel. In order to check the accuracy of the determination of the velocity by means of the pressures, two obstacles of small thickness were placed on the walls of the test chamber and the angle measured between the shock waves to which the obstacles gave rise. The check was found to be favorable. Having made this preliminary check, the forces were then measured with the new balance previously described (reference 1). With this balance the three components of lift, drag, and pitching moment could be easily obtained.

The airfoils spanned the tunnel and were connected to the balance outside the test chamber. The support across the test chamber was obtained by means of openings which interrupted the continuity of the walls and permitted a small play of the airfoil. The two parts put in communication by the opening were maintained at the same pressure so as to prevent any leakage flow at the ends. All the measurements were repeated many times so as to eliminate the experimental errors as far as possible.

The pressure distribution along the wing section was determined with suitably constructed airfoils. These airfoils, which likewise spanned the tunnel, were connected to two movable windows set in the plane tunnel walls exposed to the flow. The pressure orifices located on the top and bottom wing surfaces were staggered spanwise so as to avoid mutual disturbance on each other. The orifices communicated through very thin tubes enclosed within the wing with the tubes of a multiple tube manometer externally located. The pressure readings were photographically recorded.

For the optical observations a provisional striometrical apparatus was employed, since the final form of the apparatus has not yet been decided upon. This apparatus is far from perfect and, moreover, reproduces in the photographs, numerous streaks due, not to aerodynamic phenomena but to optical imperfections in the glass of the tunnel windows. These defects, however, which can easily be traced to their source, do not mask the aerodynamic phenomena, which still show up with sufficient clearness.

TEST RESULTS

A) Results of the Aerodynamic Measurements

The force measurements were conducted on the following four wing sections (fig. 1):

Section G.U.2, consisting of two arcs of circles with radius equal to 2.5 times the chord. The thickness is 10 percent of the chord while the angle made with the chord at the leading and trailing edges is 11° 20'.

Section G.U.3, consisting of a circular arc and a straight line. The radius of the circle is 1.46 times the chord, and the thickness is 8.8 percent of the chord while the angle at the leading and trailing edges is 20°.

Section G.U.4, consisting of three straight lines. This airfoil, which is symmetrical with respect to the normal to the chord, together with an equal airfoil, constitutes a biplane of the "Busemann" (reference 2) type, on which experimental investigations are being planned. The thickness is 6.3 percent of the chord. The angle at the leading and trailing edges is 7°.

Section G.U.5, consisting of four straight lines. The thickness is 10 percent of the chord and is divided in the ratio of 6 percent thickness above the chord line and 4 percent below the chord line. The maximum thickness is at 56 percent of the chord. The sides at the leading edge form, with the chord, an angle of 6° 10' above the chord line, and 4° 10' below; while the other two sides form angles of 7° 50' and 5° 10', respectively.

For all the airfoils, the aerodynamic characteristics were also computed theoretically, and the curves plotted (shown dotted) together with those obtained experimentally. The method used for the computation of the characteristics of sections G.U.2 and G.U.3, is that given by Busemann in his paper before the Volta Congress in 1935, while the shock characteristics of the other sections were computed by the exact formulas of L. Crocco (reference 3), by which were determined the subsequent expansions and the resulting forces.

The experimental results are presented on figures 2 to 9, inclusive; the aerodynamic coefficients C_p, C_r, and C_p/C_r computed by the standard formulas:

$$\tfrac{1}{2}C_L = C_p = \frac{P}{\rho\ S\ V^2}; \quad \tfrac{1}{2}C_D = C_r = \frac{R}{\rho\ S\ V^2}$$

being plotted against the angle of attack. There is also given as a function of the lift coefficient, the pitching moment computed from the formula:

$$C_m = \frac{M}{\rho\ S\ V^2\ l}$$

where M is the moment measured about the leading edge, and l is the profile chord. The angles of attack are referred to the chord defined as the line joining the trailing and leading edges of the airfoil.

From an examination of the experimental results, the following conclusions can be drawn:

1) The shape of the curve of the lift coefficient against angle of attack is practically rectilinear.

2) The lift curve slope $d\ C_p/d\alpha$ has a very low value.

3) For even high angles of attack, in some cases angles of attack of 28° were obtained (figs. 2 and 6); no maximum value of the lift coefficient C_p is obtained.

4) When the deflection of the flow at the edge is above the maximum for which, according to the theory, the shock wave can still adhere to the edge and beyond which separation occurs, it is observed that the lift curve

ceases to be straight and the slope $dC_p/d\alpha$ changes its value. This phenomenon is observed on all the curves with notable agreement with the values given by the theory which predicts the breaking away of the shock wave for a compression deflection of about 25° for $M = 2.13$ and about 20° for $M = 1.85$.

5) On computing the theoretical values of C_p as a function of the angle of attack, it is found that the theoretical curve diverges from the experimental. The two curves differ in their slopes and in general in the value of the angle of attack at zero lift. In all cases the theoretical value of $dC_p/d\alpha$ is greater than the experimental.

6) The shape of the drag coefficient curve is the same as the theoretical curve but they differ in specific values. Comparing the theoretical values (dotted curves) with the test values, differences are noted which vary with change in angle of attack. For low angles of attack the theoretical curve gives values below the experimental in figures 2 and 5, approximately equal values in figures 3, 4, 6, 8, 9, and higher values in figure 7.

7) With increase in the angle of attack either in the positive or negative region, it is observed that $dC_r/d\alpha$ is always greater for the theoretical curve as compared with the experimental curve, so that at a certain point the experimental values pass above the theoretical for all the sections. This trend* of the curves appears somewhat strange at first sight, since in the theoretical curves there is not included the friction drag which would raise the theoretical curve and hence would increase the positive differences between the theoretical drag coefficient and the experimental.

8) The variation of the moment coefficient as a function of the lift coefficient is also practically rectilinear at the low angles of attack, while it tends to curve in the sense of increasing dC_m/dC_p at the higher angles of attack.

9) The maximum experimental value of C_p/C_r is less than that theoretically computed.

B) Results of the Pressure-Distribution Tests

As has been said, the pressure-distribution measurements were carried out only on the airfoils G.U.2 and G.U.3. For the other airfoils, corresponding models were not suitable for this purpose, hence the tests were postponed to a later period. Tests were conducted at the two Mach numbers, 1.85 and 2.13, and the results are presented on figures 10, 11, 12, and 13 - the full lines giving the experimental, and the dotted lines the theoretical values. It is to be noted that the theoretical values with respect to the low-pressure side of the airfoil for which the deflection due to the other side is above the maximum for which the shock wave can still adhere, were also plotted. After a wave is separated from the section, the values obtained no longer have any precise meaning. However, since they appear to agree sufficiently well with the experimental values, they also were plotted in order that a comparison could be made.

The curves are plotted nondimensionally, the values of the pressures being divided by the dynamic pressure $q = \frac{1}{2} \rho V^2$, where V and ρ are the velocity and density of the undisturbed flow in the test chamber.

The negative pressures are plotted above the base line and the positive pressures below; the static pressure in the test chamber being taken as the origin of pressures. The experimental values are distinguished on the curves by two different symbols - the circles referring to orifices on the upper wing surface, and the dots to orifices on the lower wing surface. For section G.U.2, which is symmetrical with respect to the chord, measurements were taken for alternately positive and negative angles, so that any possible experimental dissymmetry might be checked.

On the subjoined tables are given in millimeters of mercury the values of $q = \frac{1}{2} \rho V^2$, p the static pressure in the test chamber, and the pressure variations along the wing chord with respect to the ambient static pressure. On the graphs, the side of one of the squares represents 1/15 of q.

From an examination of the curves, the following conclusions may be drawn:

1) The computation of the pressure jump through a shock wave gives values agreeing well with those extrapolated from the experimental values up to the leading edge.

2) When the angle of deflection is such as to determine an expansion, the computation of the latter from the deflecting angle by the Prandtl formulas, gives values somewhat above the experimental values. This disagreement, to which we shall return later on, might perhaps be attributed to the fact that the edge, although tapered and quite sharp, cannot coincide with the theoretical "corner" and therefore creates a small, though definite, disturbance. The reason, however, is not entirely clear, and further investigation is required.

3) Comparison of the successive expansion along the upper and lower wing surfaces with that calculated by the formulas of expansion about a corner, shows a definite agreement in the entire experimental range except in a particular region which will be discussed under 4) below. Even excluding the latter region, the agreement is not perfect, and a careful examination reveals a more or less regular deviation from theory. It is seen, for example, that while the expansion curves which start from a negative pressure are practically parallel to the computed curves when the expansion begins from a positive pressure - that is, when it follows a shock wave - the curvature of the experimental curve is in general less accentuated than that of the computed curve and, in particular, the initial slope of the former is in absolute value somewhat above that of the computed curve. These phenomena show up more clearly in the case of the plano-convex section G.U.3, which has a greater curvature than the symmetrical section G.U.2.

This divergence is probably due to the imperfection in the method of computation used. In computing the expansion about the wing section, the case has been considered as analogous to the expansion about a corner. In order that the analogy may be perfect, however, it would be necessary that the Mach lines which originate at the contour, should continue undisturbed to infinity as in the theoretical case of Prandtl. This happens only if the expansion is not preceded, as in our case, by a shock wave which modifies the conditions. This fact has been pointed out by L. Crocco (reference 4), who has shown that if the expansion is preceded by a shock wave, the phenomenon changes and the simple scheme assumed by us for the computation is no longer applicable because the Mach lines then interfere with the shock wave, curving the latter and being in part reflected, and then returning to the surface contour; while behind the shock wave, since the latter is not plane, there is a vorticity which further complicates the phenomenon.

There does not exist at present any theory that permits computation of the entire expansion, taking into account all of the above factors. The only indication of their nature is that given by L. Crocco, who - in the second of the papers referred to, starting out from exact formulas and considering the phenomenon as a whole - has computed the pressure gradient at which the expansion following the shock wave, begins. The values of the pressure gradient thus obtained are greater than those computed by the scheme employed by us (see, for example, fig. 14), and hence more closely approach the experimental values. The absence, however, of test points very close to the origin, does not permit ascertaining up to what point the experimental curve agrees with the theoretical. We shall return to this subject in later tests.

4) When, during the expansion, the pressure reaches absolute values less than the ambient pressure, it is observed with perfect agreement that the expansion does not proceed up to the trailing edge, but that at a certain point there is a sudden pressure increase, after which the pressure remains practically constant, or begins to decrease. This sudden drop in the expansion curve makes the theoretical curve differ markedly from the experimental curve in this region, and for this reason brings out the phenomenon, namely, that in the supersonic region the lift is, for the most part, contributed by the positive pressures rather than by the negative.

5) The phenomenon referred to above occurs only when pressures less than the ambient are attained, and vanishes if, by varying the angles of attack, the pressure is increased until values equal to or greater than the ambient pressure, are reached.

6) The point of the wing at which sudden recompression occurs, is not fixed but shifts along the wing chord. As regards its position, the following may be observed:

a) The position at which the sudden drop in the curve occurs, depends on the angle of attack of the wing and shifts from the trailing to the leading edge if the angle of attack is varied so as to increase the expansion on the wing surface under consideration.

b) If, for the same wing and same angle of attack, the pressure curves referring to different Mach numbers are compared, there is observed a certain correspondence in the point of discontinuity, such as to lead to the supposition that the position of this point is unaffected by the Mach number.

c) If the pressure curve referring to different sections for which the angle of attack is such that the angle of inclination, with respect to the wind direction, of the tangent at the trailing edge is the same, a certain agreement is found also in the values of the inclination of the tangent to the profile at the point where the expansion ceases. These observations are only of an indicative character, since the point in question is not well defined on account of the separation of the test points, but they lead to the supposition that the sudden recompression not predicted by the theory is connected with the deflection that must occur at the trailing edge and with the resulting shock phenomenon.

7) On integrating the curves and computing C_p, values are found that agree with those obtained from the force measurements.

C) Results of the Optical Tests

The optical tests were conducted on three different airfoils: two similar to section G.U.3, and one similar to G.U.2. The first two, therefore, are plane on one side and circular on the other, but differ from section G.U.2 in the percent maximum thickness, and hence in the dihedral angle at the leading and trailing edges. The third section is symmetrical with a circular arc, but also differs in its thickness from section G.U.2. The sections tested are G.U.6, G.U.7, and G.U.8 (fig. 1).

The reason that the same models on which the force measurements were made were not used for the optical tests, is that for the latter tests the airfoils had to be mounted between two glass plates 40 centimeters apart while for the force measurements, the airfoils spanned the tunnel and hence were of greater dimensions. For this reason, having the above three models available at the desired lengths of 40 centimeters, it was preferred not to cut down sections G.U.2 and G.U.3 to conduct the tests on these. For the other two sections, two other models are under construction, suitable for the optical and the pressure-distribution tests.

The tests on these airfoils were conducted by mounting them on two supports rigidly fixed to the lower surface by means of screws (fig. 15). The supports, connected to two streamlined struts, permitted the variation of the angle of attack. A great number of optical observations were made; hence only a few of the most interesting are presented (figs. 16 to 47). From observation of these photographs, the following conclusions may be drawn:

1) On the leading edge, when the flow undergoes a pressure deflection, there is a well-defined shock-wave formation.

2) The value of the wave angle with respect to the horizontal, to the approximation permitted in measuring this angle from the photographs, agrees with the theoretical value computed on the basis of the flow deflection.

3) At the leading edge, whenever the flow undergoes a deflection of expansion, an expansion is observed in accordance with the theory of deflection about a corner (figs. 30, 31, 39). The photographs also appear to reveal the existence of a small shock wave (compression) that precedes the expansion. This phenomenon, whose existence requires further confirmation, would explain the divergence indicated under 2) of the preceding section.

4) Also at the trailing edge there exists either a shock wave or a rapid expansion, according to whether the flow undergoes a deflection of compression or expansion.

5) On the side of the wing on which there is expansion, and which should therefore have a compression shock at the trailing edge, there is observed in every case a phenomenon not predicted by the theories, namely, that before reaching the trailing edge there is a sudden pressure increase, well brought out in the photographs, by a shock wave which separates two regions of very different luminosity (figs. 18 to 27, 30 to 37, 40 to 46). Associated with this phenomenon is another, namely, that at the point at

which there is this sudden pressure jump, where the flow no longer adheres to the contour but from that point on a wake of almost rectilinear shape is separated. The shock wave corresponding to the trailing edge is still generated, however, though it does not originate at the profile but outside the wake. From checks made, with the approximation permitted by the photographic data, it is found that for the point at which the wake separates the same considerations apply as those under 6) of the preceding section for pressure-distribution measurements. It is evident that the separation of the wake and the sudden change in the pressure are connected and represent a single phenomenon, of which the drop in pressure is the effect while the separation is the cause.

6) This phenomenon does not present itself when an expansion occurs at the trailing edge.

7) With increase in the angle of attack the compression shock on the upper side of the wing at the leading edge becomes greater and the compression deflection increases. When, according to the theory, it is no longer possible to have an adhering shock on the surface, it is observed that the shock becomes stronger while the shock wave assumes a very curved shape and begins to move away from the leading edge (figs. 16, 17, 18, 19, 20, 28, and 29).

CONCLUSIONS AND HYPOTHESES AS TO THE POSSIBLE CAUSES OF THE OBSERVED PHENOMENA

On comparing the three series of experimental results, the following conclusions are arrived at:

1) The phenomenon of compression shock on the leading edge follows, even quantitatively, the predictions of the theory with good approximation.

2) Also the phenomenon of the expansion about the leading edge follows the theoretical prediction. Some reservation can be made with regard to the presence of a slight shock wave preceding the expansion and likewise starting out from the leading edge - this shock wave not being predicted by any existing theory. This anomaly will be the object of further investigations.

The two phenomena under 1) and 2) above, are localized phenomena, and it is seen that together the localized phenomena correspond with sufficient approximation to the theoretical predictions.

3) The nonlocalized expansion after either of the phenomena, 1) and 2) above, follows qualitatively that computed by the approximate existing theory. The quantitative divergence appears in part due to the inexactness of the theory. According to the exact theory of L. Crocco, however, the initial pressure gradient of the expansion has a value which would give the pressure curve a shape more closely approaching the experimental curve than that computed by the approximate theory.

4) Preceding the expansion, when the pressure on the airfoil becomes less than the ambient pressure, a phenomenon appears - not predicted by the theories thus far developed - which leads to a marked divergence of the theoretical pressure curve from the actual.

5) Since the pressure distribution along the wing section varies, the resulting forces and also the aerodynamic coefficients vary. Since in the neighborhood of the trailing edge the negative pressure on the upper wing surface is considerably smaller than the theoretical, and often the positive pressure on the lower surface is also smaller, the components normal and parallel to the chord are also smaller. The values of the coefficients C_p and C_r should therefore be lower since the first is essentially associated with the normal component while the second depends on the variation of the two components. It is therefore not possible, on the basis of these theories, to obtain accurately the aerodynamic characteristics of the airfoils.

6) The cause of the disagreements between theory and experiment is probably to be ascribed to the fact that all theories neglect the friction, and therefore the formation, of a boundary layer on the wing surface. Such a boundary layer may considerably modify the phenomena because it creates a region of adhering flow where the speed is below that of sound, so that the physical laws are different from those holding for the supersonic region. The presence of a boundary layer may therefore modify the conditions of the fluid flow, giving rise to phenomena different from those predicted by a simplified theory. Dis-

agreements, moreover, due to the presence of such boundary layer, have already been predicted and clearly formulated, although no complete theory has as yet been developed. The subject had already claimed the attention of Professor Ackeret at the Volta Congress of 1935, and more recently of Professor L. Crocco, who entertained some doubts as to the compatibility of the assumption of absence of viscosity in supersonic flows with the existence of a boundary layer.

The doubts expressed by Professor L. Crocco referred particularly to the case where the flow after expanding, for example, along the upper wing surface until attaining a supersonic speed, should undergo a sudden deflection. The theory in this case shows that such deflection cannot take place except through a shock wave, which also produces a sudden pressure increase. In the ideal case of a fluid without viscosity, the shock wave would originate on the body contour and at the trailing edge. The presence of the boundary layer in this case, however, considerably alters the flow conditions. In passing from the region outside to the region inside the boundary layer, the shock wave always encounters decreasing velocity; and since the pressure increase ultimately occurs at the expense of the kinetic energy of the gas, where this energy goes below a certain value it is no longer possible for a shock wave to be formed that generates the same pressure increment that exists outside the boundary layer. On further approaching the surface of the body the velocity becomes supersonic, subsonic the existence of the shock wave is no longer possible, and the same pressure jump as the external cannot be established. It is thus seen that the existence of the boundary layer not only prevents the shock wave from extending to the surface of the body but, moreover, makes it impossible in the neighborhood of the surface, on the assumption of regular flow in the ideal case, for the expanded gas to attain the pressure downstream of the section approximately equal to the ambient static pressure. This leads to the conclusion that in the actual case the phenomena are considerably modified. The pressure-distribution measurements and flow photographs have clearly brought to light the real nature of the phenomenon and definitely indicate the existence of a separation of the flow which, by deviating the stream, results in a first shock wave (clearly visible on the pressure-distribution curves, figs. 10, 11, 12, 13, and on the photographs, figs. 16, 17, etc.), while the principal shock wave that should start out from the trailing edge is displaced behind the edge on the contour of the separated wake (figs. 16, 17, etc.).

7) From the above, it may be concluded that in the exact evaluation of the characteristics of a wing profile at supersonic speed, the viscosity phenomena cannot be neglected. In this respect, the gas dynamic phenomena differ from the aerodynamic phenomena at low speed, for which the friction appreciably influences only the drag while the lift is practically independent of it up to the critical angle of attack. At the present stage of our knowledge of gas dynamics, no airfoil theory exists that takes account of the viscous forces. It is thus evident that more profound experimental investigation, in addition to providing data of direct engineering application, may provide the basis for the construction of a more complete theory.

Translation by S. Reiss,
National Advisory Committee
for Aeronautics.

REFERENCES

1. Ferri, A.: Investigations and Experiments in the Guidonia Supersonic Wind Tunnel. T.M. No. 901, N.A.C.A., 1939.

2. Busemann, A.: Aerodynamischer Auftrieb bei Ueberschallgeschindigkeit. Atti del Convegno di Scienze fisiche, matematiche e naturali della Reale Accademia d'Italia - Fondazione Volta, 1935.

3. Crocco, L.: Singolarita della corrente gassosa iperacustica nell'interno di una prova a diedro. L'Aerotecnica, vol. XVII, no. 6, June 1937.

4. Crocco, L.: Una nuova funzione di corrente per lo studio del moto rotazionale dei gas. Rendiconti della R. Accademia dei Lincei, vol. XXIII, ser. VI, Feb. 1936. (See also reference 3.)

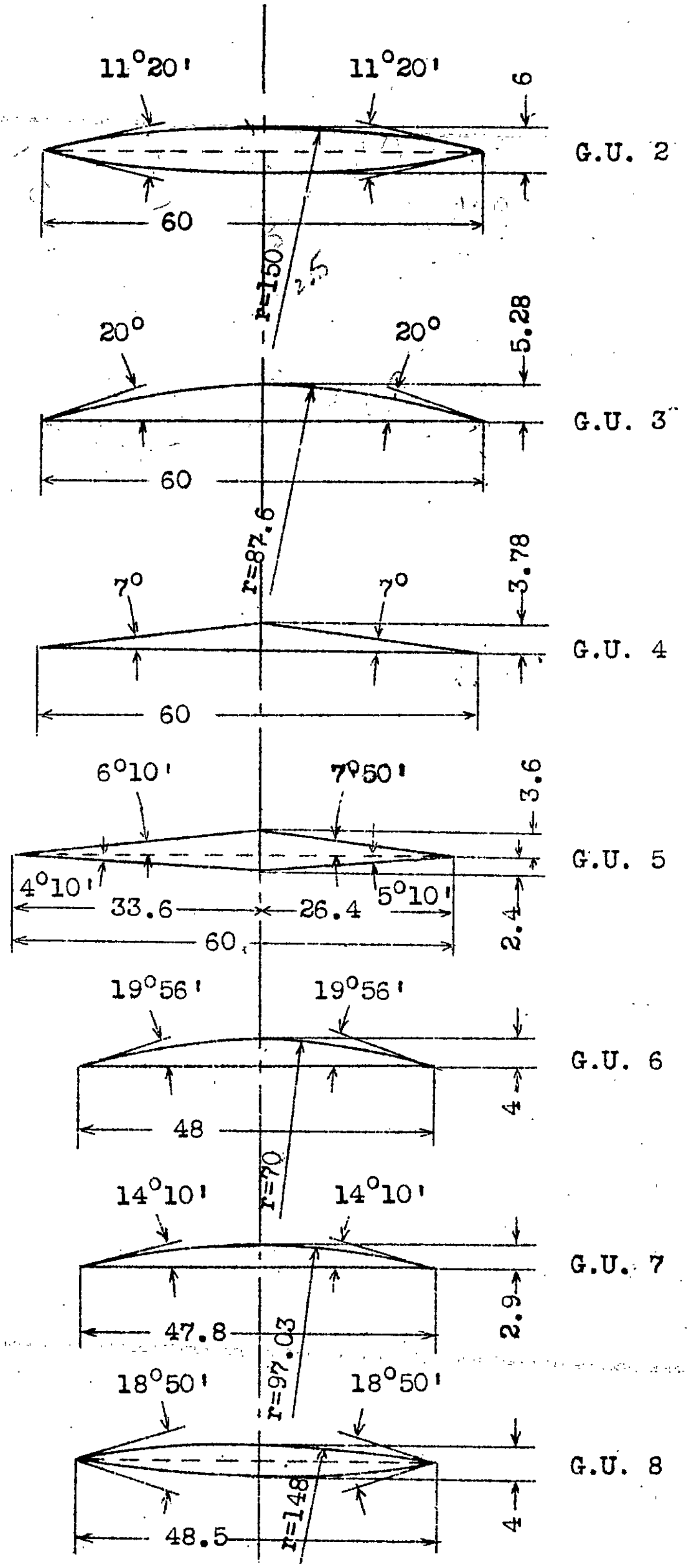

Figure 1.- Geometric characteristics.

α°	− 10°		− 8°		− 6°		− 4°		− 2°		0°		2°	
100 C_p	−16,2	−16,3	−13,2	−12,8	− 9,8		− 6,0	− 6,1	− 3,5	− 3	0	− 0,1	2,7	3,2
100 C_r	4,90	4,92	3,70	3,75	2,83		2,20	2,20	1,86	1,87	1,76	1,75	1,88	1,90
100 C_m	− 5,7	− 5,1	− 5,1	− 4,6	− 3,2		− 1,8	− 2,0	− 0,8	− 0,6	− 0,1	+ 0,2	0,7	1,4

α°	4°		6°		8°		10°		12°		14°		16°	
100 C_p	6,2	6,3	9,5	9,8	13,1	13,3	16,7	16,6	20,5	20,3		23,8	26,8	27,5
100 C_r	2,09	2,23	2,85	2,83	3,75	3,73	4,90	4,92	6,51	6,79		8,35	10,45	10,43
100 C_m	1,9	2,2	3,5	3,8	4,9	5,1	6,4	6,6	7,0	7,8		9,7	10,5	10,9

α°	18°		20°		22°		24°		26°		28°
100 C_p	30,3	30,9	33,7	34,4		37,5	39,5	41,2	44,8	44,0	48,1
100 C_r	12,82	13,09	15,24	15,40		17,81	20,60	20,85	23,45	23,30	26,30
100 C_m	13,2	13,3	14,3	15,3		17,5	18,5	20,9	22,5	22,4	25,1

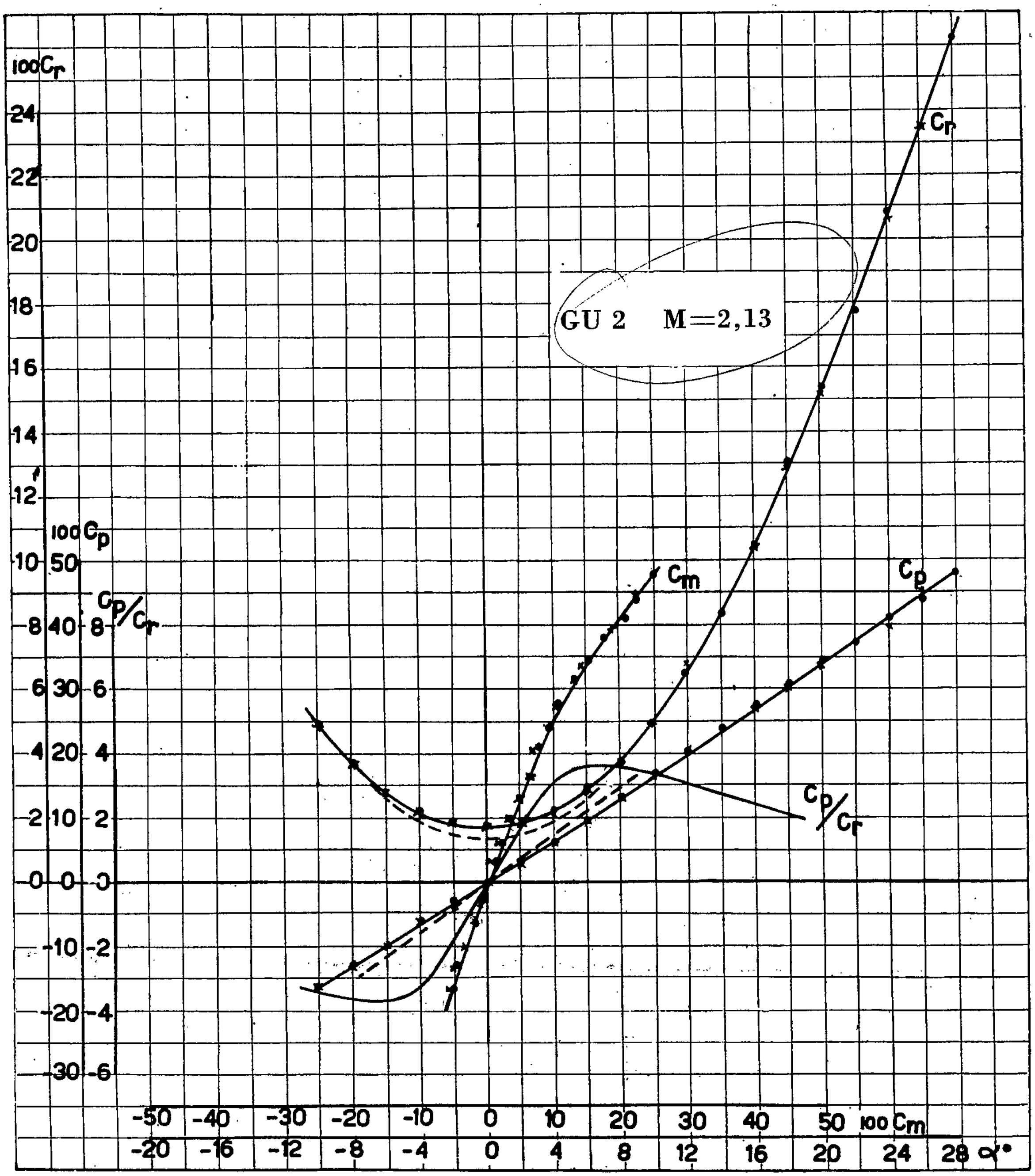

Fig. 2

α°	−10°		−6°		−4°		−2°		0°		2°		4°	
100 C_p	−19,5		−13	−13,5	−10,5	−10,4	− 6,5	− 6,0	− 3,5	− 3,5	0,1	0,3	3,5	4,1
100 C_r	7,02		4,42	4,43	3,40	3,37	2,65	2,70	2,22	2,23	2,13	2,12	2,18	2,21
100 C_m	− 5,4		− 3,3	− 3,2	− 2,5	− 2,6	− 1,2	− 1,5	0,5	0,4	2,1	2,0	3,6	3,7

α°	6°		8°		12°		16°		18°		20°		22°	
100 C_p	7,4	8,1	11,1	11,5	18,2	19,1	26,4	26,2	31,6	30,2	33,5	34,4	39,1	
100 C_r	2,53	2,62	3,10	3,25	5,28	5,45	8,85	9,08	11,61	11,79	14,39	14,21	17,55	
100 C_m	5,5	5,5	7,0	7,2	10,2	11,0	14,5	14,9	18,7	17,2	18,5	19,5	23,0	

α°	24°
100 C_p	44,5
100 C_r	21,30
100 C_m	26,5

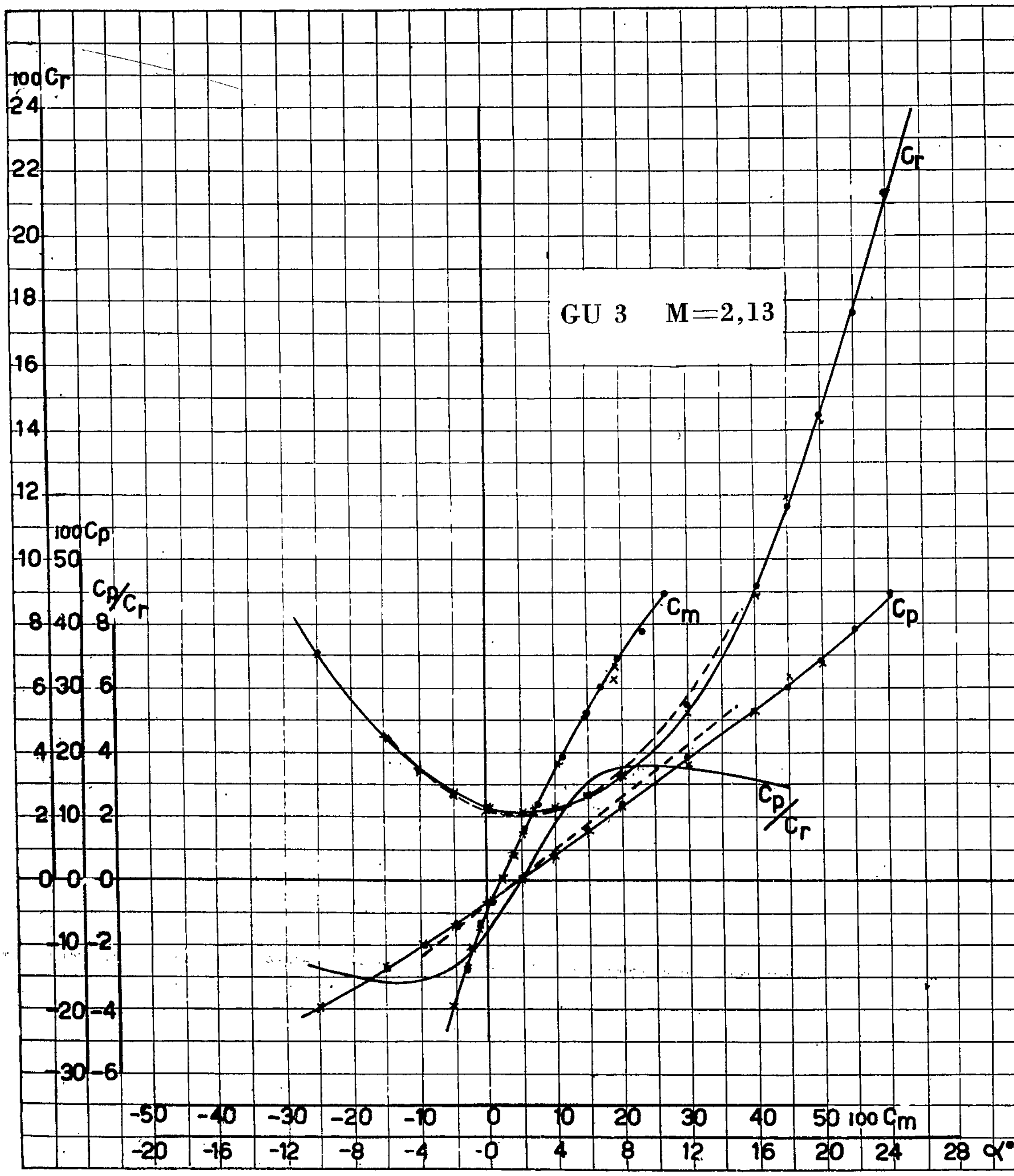

FIG. 3

α^0	-14^0	-12^0	-10^0	-9^0	-8^0	-7^0	-6^0	-4^0	-3^0	-2^0
$100\,C_p$	−24,0	−20,6	−17,4	−15,7	−13,8	−12,3	−10,9	− 7,6	− 5,8	− 4,2
$100\,C_r$	7,75	6,13	4,65	4,31	3,98	3,02	2,51	1,77	1,42	1,20
$100\,C_m$	− 8,5	− 7,2	− 6,3	− 5,5	− 4,6	− 4,1	− 3,7	− 2,5	− 1,8	− 1,0

α^0	-1^0	0^0	1^0	2^0	3^0	4^0	5^0	6^0	7^0	8^0
$100\,C_p$	− 2,5	− 0,74	0,9	2,4	4,2	5,9	7,5	9,1	10,8	12,5
$100\,C_r$	1,02	0,91	0,82	0,82	0,85	1,01	1,20	1,42	1,75	2,14
$100\,C_m$	− 0,4	0,0	0,9	1,5	2,1	3,0	3,5	4,1	4,7	5,6

α^0	9^0	10^0	12^0	14^0	16^0	18^0	20^0	22^0
$100\,C_p$	14,3	16,0	19,2	22,4	25,7	29,0	32,4	36,5
$100\,C_r$	2,58	3,15	4,40	5,93	7,78	9,98	12,52	15,46
$100\,C_m$	6,2	7,1	8,8	10,9	13,0	15,2	17,8	22,3

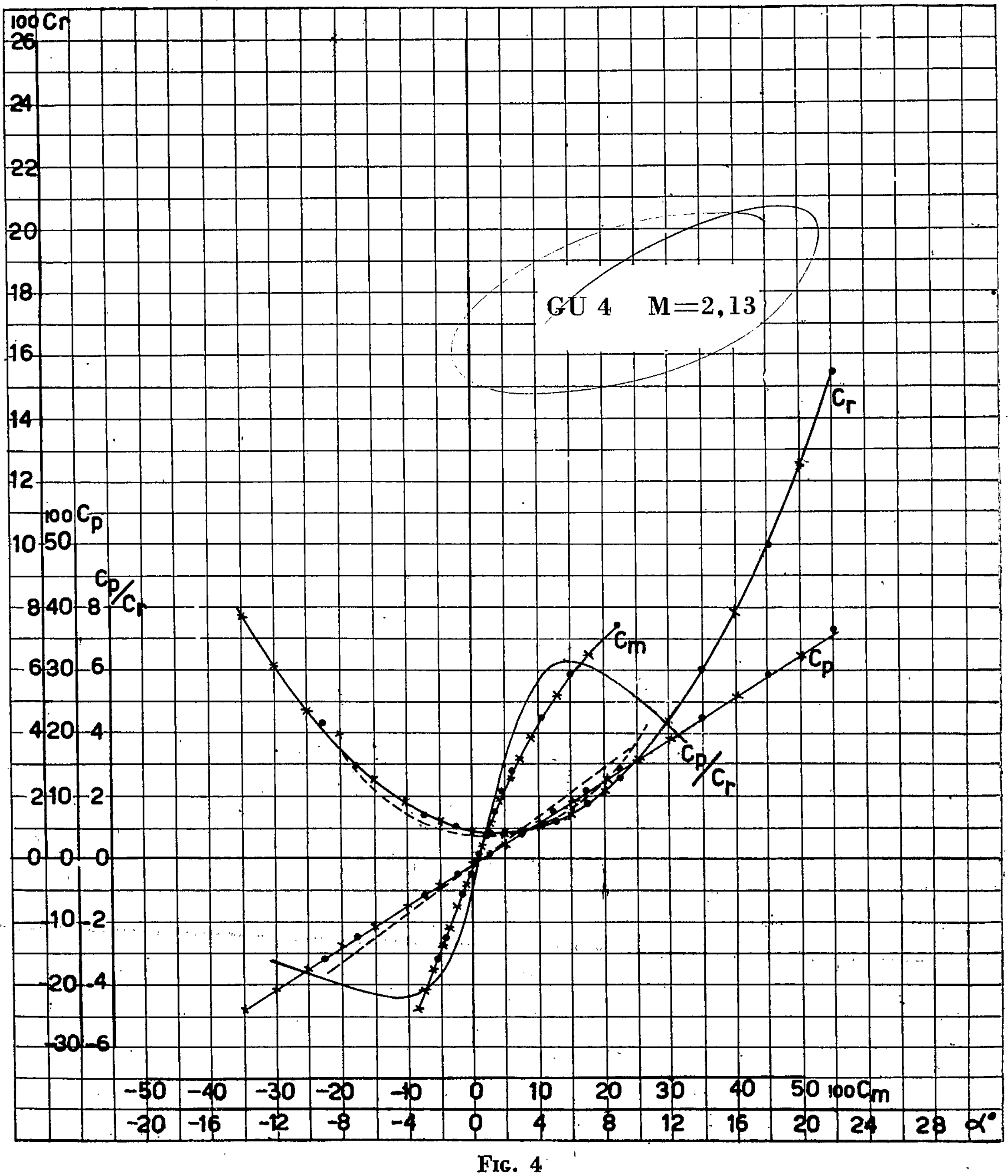

Fig. 4

α°	—18°	—16°	—14°	—12°	—10°	—8°	—7°
100 C_p	—28,2	—25,0 —25,7	—22,0	—18,6 —18,7	—15,9	—12,2 —12,5	—11,2
100 C_r	—12,98	10,52 10,62	8,22	6,31 6,45	4,88	3,80 3,79	3,22
100 C_m	—10,9	— 9,2 — 9,4	— 8,0	— 6,9 — 7,0	— 4,8	— 3,6 — 3,7	— 3,4

α°	—6°	—5°	—4°	—3°	—2°	—1°	0°
100 C_p	— 9,7 — 9,6	— 7,7	— 6,6 — 6,7	— 5,0	— 3,4 — 3,5	— 2,1	— 0,4 — 0,5
100 C_r	2,74 2,99	2,59	2,12 2,29	2,05	1,83 1,85	1,72	1,68 1,65
100 C_m	— 2,8 — 2,6	— 2,1	— 1,6 — 1,7	— 1,1	— 0,7 — 0,6	— 0,1	0,4 0,3

α°	1°	2°	3°	4°	5°	6°	7°	8°
100 C_p	1,3	3,0 2,5	4,9	6,5 5,6	8,0	9,6	11,3	12,4' 12,9
100 C_r	1,69	1,74 1,75	1,89	1,9 2,0	2,25	2,51	2,91	3,29 3,3
100 C_m	0,7	1,7 1,4	2,1	2,9 2,6	3,6	4,2	4,7	4,9 5,1

α°	+10°	12°	14°	16°	18°	20°	22°
100 C_p	16,8	20,4 20,1	23,7	28,1 26,9	31,0	34,2 34,6	38,1
100 C_r	4,49	5,8 6,29	7,38	9,48 9,28	11,80	14,25 14,39	17,50
100 C_m	5,4	8,9 8,7	9,1	12,2 11,7	14,1	16,4 16,4	19,0

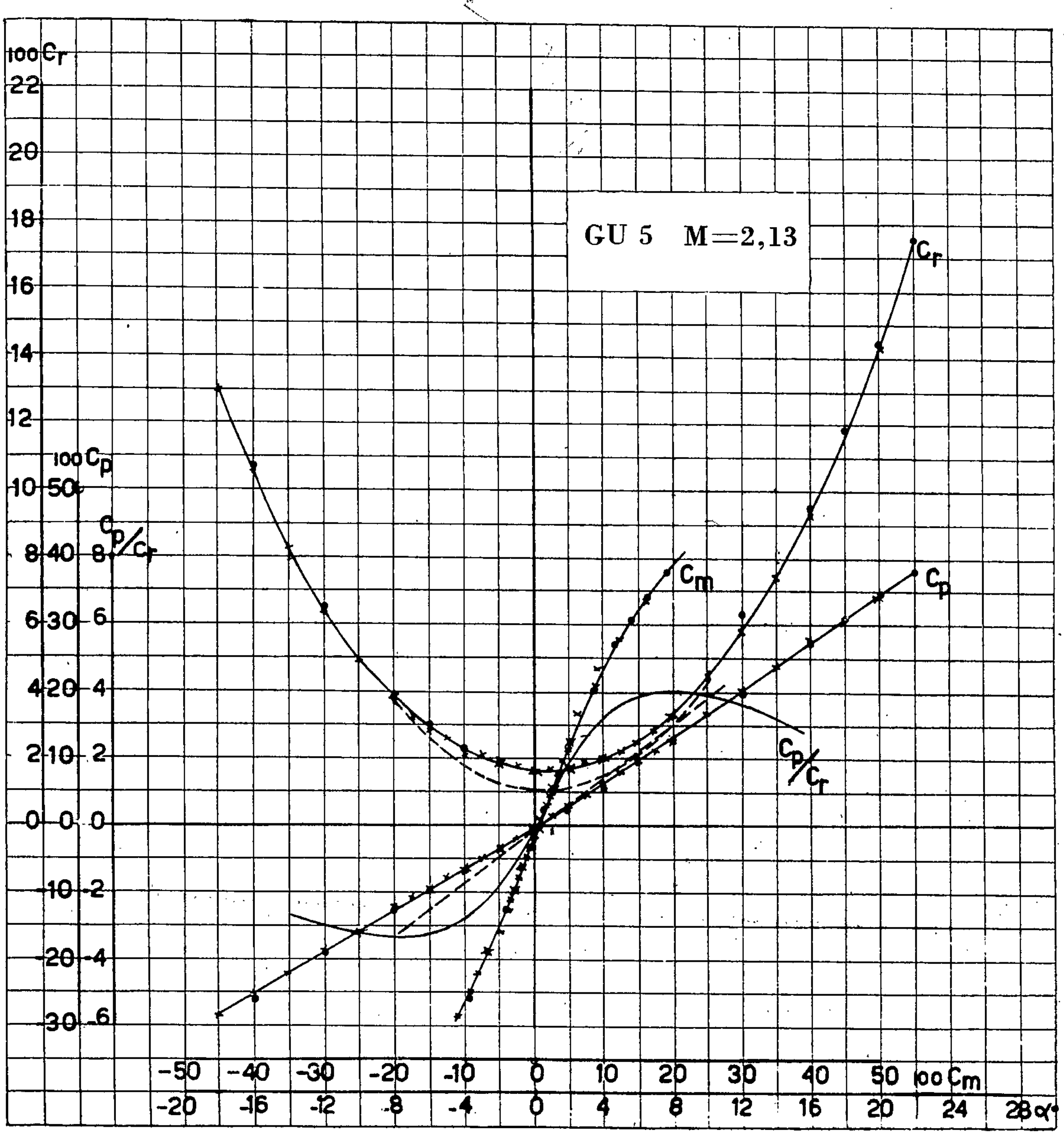

Fig. 5

α°	−24,8°		−22,8°		−20,8°		−18,8°		−16,8°		−14,8°		−12,8°	
100 C_p	−40,0		−37,5		−34,5		−32,3		−28,5		−25,8	−25,6	−22,0	−23,1
100 C_r	20,30		17,31		15,01		13,15		10,51		8,65	8,92	6,50	6,91
100 C_m	−20,2		−13,		−16,2		−13,2		−13,1		−11,6	−11,1	−9,6	−9,2

α°	−10,8°		−8,8°		−7,8°		−6,8°		−5,8°		−4,8°		−3,8°	
100 C_p	−18,8	−18,8	−15,5	−13,5	−13,6		−11,5	−12,02	−10,0	−10,1	−8,51	−8,30	−6,5	−6,2
100 C_r	5,22	5,45	4,13	4,70	3,62		3,20	3,20	2,72	2,73	2,38	2,41	2,12	2,19
100 C_m	−8,3	−7,2	−6,2	−6,5	−5,8		−5,0	−5,4	−4,2	−4,0	−3,5	−3,5	−2,5	−2,7

α°	−2,8°		−1,8°		−0,8°		0,2°		1,2°		2,2°		3,2°	
100 C_p	−4,5	−4,6	−3,2	−3,2	−1,4	−1,4	0,3	0,4	1,9	2,0	3,8	3,7	5,5	5,6
100 C_r	1,90	1,91	1,75	1,81	1,71	1,80	1,69	1,79	1,73	1,73	1,85	1,84	2,01	2,09
100 C_m	−2,0	−2,1	−1,2	−1,5	−0,5	−0,7	0,2	0,1	0,7	0,8	1,7	1,6	2,2	2,3

α°	4,2°		5.2°		6,2°		7,2°		9,2°		11,2°		13,2°	
100 C_p	7,1	7,0	9,0	8,9	11,3		12,53	12,65	16,0	15,9	19,5	19,5	23,0	21,3
100 C_r	2,31	2,35	2,65	2,64	3,00		3,61	3,60	4,35	4,51	5,79	5,99	7,40	7,41
100 C_m	3,0	3,1	3,7	3,8	4,5		4,9	5,2	6,3	6,7	8,2	8,4	10,0	10,1

α°	15,2°		17,2°	19,2°	21,2°	23,2°	25,2°	27,2°
100 C_p	24,5	26,5	29,5	32,6	35,8	38,5	40,9	42,7
100 C_r	8,61	9,40	11,45	13,52	16,01	18,52	21,22	24,60
100 C_m	11,0	11,8	13,5	15,8	17,8	19,2	20,4	22,3

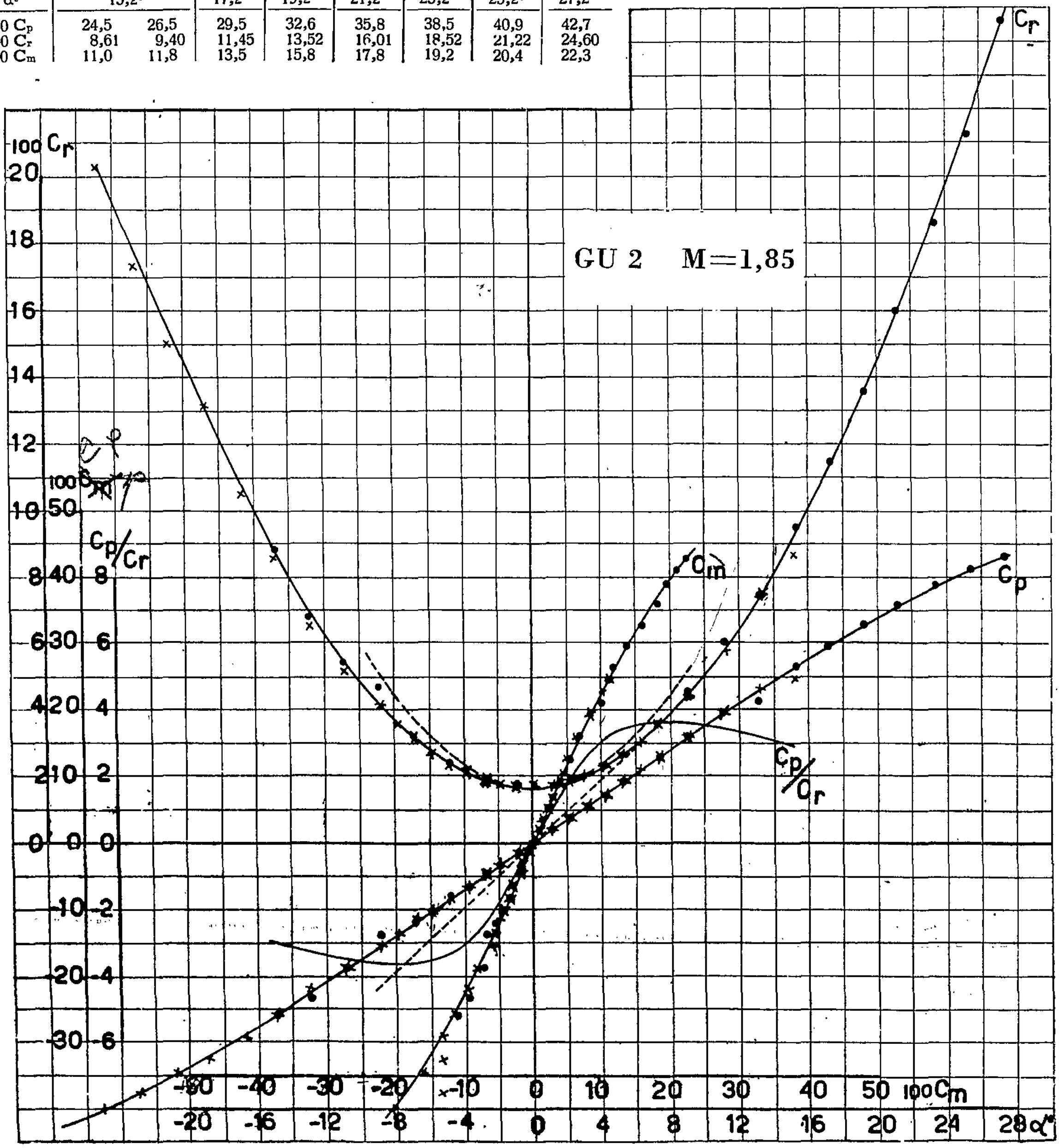

Fig. 6

α°	−20°		−18°		−16°		−14°		−12°		−10°		−8°	
100 C_p	−33,4	−32,1	−30,9	−30,4	−28,6	−28,1	−25,6	−25,4	−23,3	−23,2	−19,7	−20,4	−17,7	−16,9
100 C_r	16,45	16,10	14,31	12,79	12,29	12,01	10,45	10,1	8,85	8,55	7,31	7,15	5,89	5,72
100 C_m	−10,8	−10,1	− 9,7	− 9,1	− 8,6	− 8,1	− 7,5	− 7,7	− 6,1	− 6,5	− 4,8	− 5,3	− 3,8	− 3,5

α°	−7°		−6°		−5°		−4°		−3°		−2°		−1°	
100 C_p		−15,9	−15,2	−14,3	−13,7	−12,7	−12,1	−11,7	−10,2	− 9,6	− 8,7	− 8,1	− 6,3	− 6,2
100 C_r		5,22	4,78	4,65	4,21	4,12	3,78	3,59	3,29	3,28	2,95	2,85	2.61	2,63
100 C_m		− 3,4	− 3,1	− 3,2	− 2,3	− 2,6	− 2,0	− 1,9	− 1,5	− 1,6	− 0,9	− 1,0	− 0,1	0,5

α°	0°		1°		2°		3°		4°		5°		6°	
100 C_p	− 4,8	− 4,5	− 2,5	− 2,5	− 0,2	− 0,6	1,4	1,5	3,1	3,2	4,8	5,0	6,1	6,6
100 C_r	2,37	2,38	2,17	2,25	2,17	2,08	2,08	2,09	2,10	2,08	2,17	2,17	2,38	2,15
100 C_m	0,7	0,7	1,5	1,3	2,5	2,4	3,5	3,1	4,0	3,7	5,0	4,6	5,6	5,1

α°	7°		8°		10°		12°		14°		16°		18°	
100 C_p	8,7	8,8	10,7	10,6	14,5	13,7	18,4	17,3	22,1	21,6	24,9	25,8	29,7	30,1
100 C_r	2,58	2,59	2,91	2,89	3,91	3,72	5,05	4,95	6,58	6,34	8,02	7,95	10,30	10,25
100 C_m	6,3	6,3	7,2	6,8	8,4	8,3	10,5	10,1	12,3	12,1	13,7	14,0	16,3	16,5

α°	20°	22°	24°	26°
100 C_p	33,8	38,7	44,1	48,7
100 C_r	12,91	16,05	19,82	23,23
100 C_m	18,9	21,9	25,7	29,1

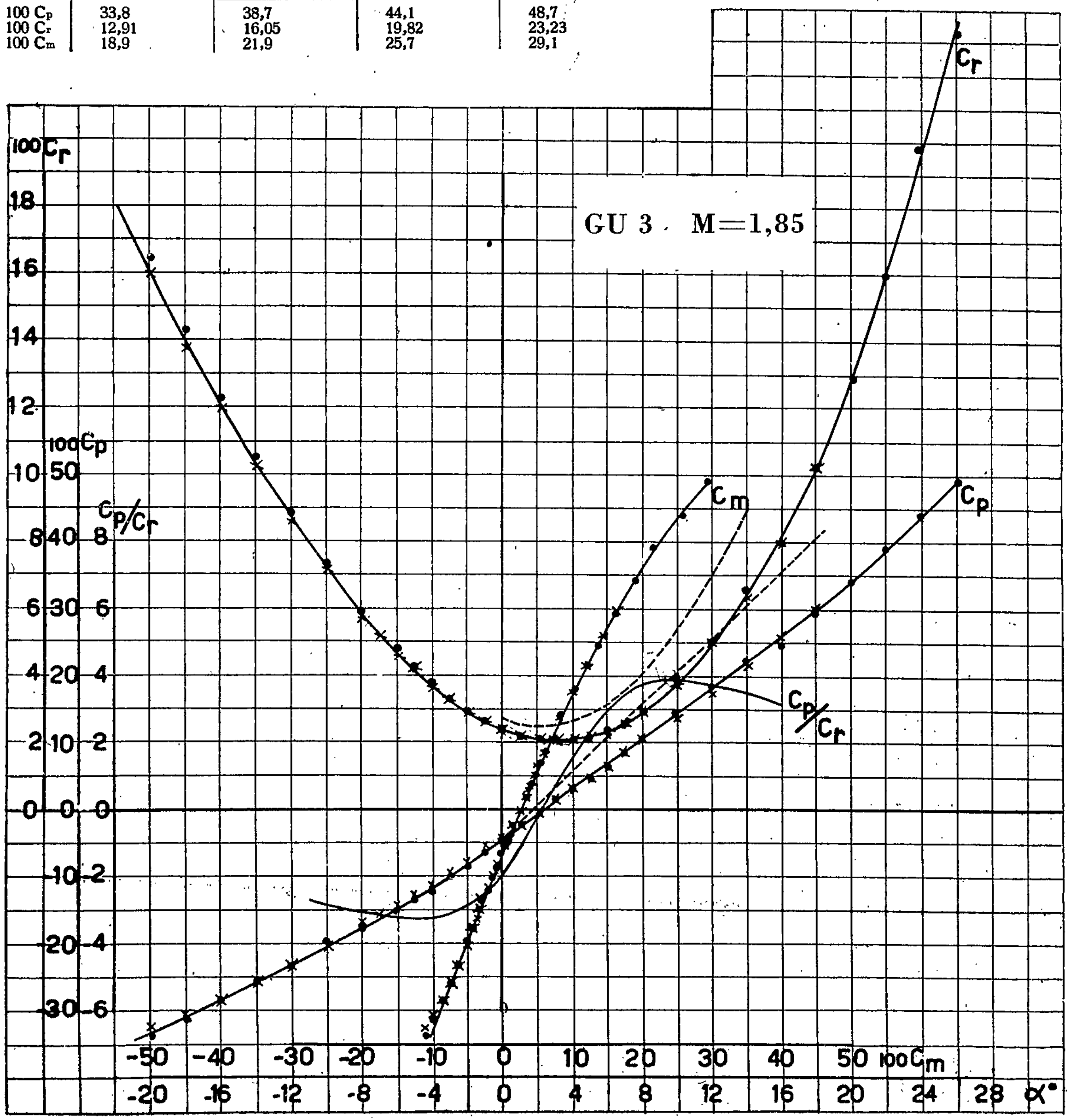

Fig. 7

α^0	— 18°	— 17°	— 15°	— 14°	— 13°	— 10°	— 9°	— 7°	— 6°	— 5°
100 C_p	—32,2	—30,7	—28,9	—27,4	—25,7	—20,2	—18,4	—14,1	—13,2	—11,3
100 C_r	13,10	11,71	10,45	9,28	8,08	5,75	4,72	3,10	3,09	2,50
100 C_m	— 5,4	— 5,8	— 5,9	— 5,6	— 5,1	— 4,4	— 3,5	— 2,5	— 2,0	— 1,8

α^0	— 4°	— 3°	— 2°	— 1°	0°	1°	2°	3°	4°	5°
100 C_p	— 9,6	— 7,50	— 6,4	— 4,0	— 2,4	— 0,5	0,9	3,1	4,7	6,6
100 C_r	2,19	1,75	1,42	1,30	1,35	1,11	1,22	1,30	1,39	1,60
100 C_m	— 1,6	— 1,0	— 0,75	0,0	0,2	0,75	1,1	2,1	2,0	2,4

α^0	6°	7°	9°	10°	13°	14°	15°	17°	18°	19°
100 C_p	8,5	10,3	14,0	15,3	21,1	22,9	24,7	28,5	30,0	32,4
100 C_r	1,87	2,18	3,01	3,59	5,52	6,30	7,11	9,25	10,55	11,62
100 C_m	3,1	3,6	4,8	4,9	6,2	7,1	7,9	9,6	10,8	13,3

α^0	20°
100 C_p	33,8
100 C_r	13,19
100 C_m	14,9

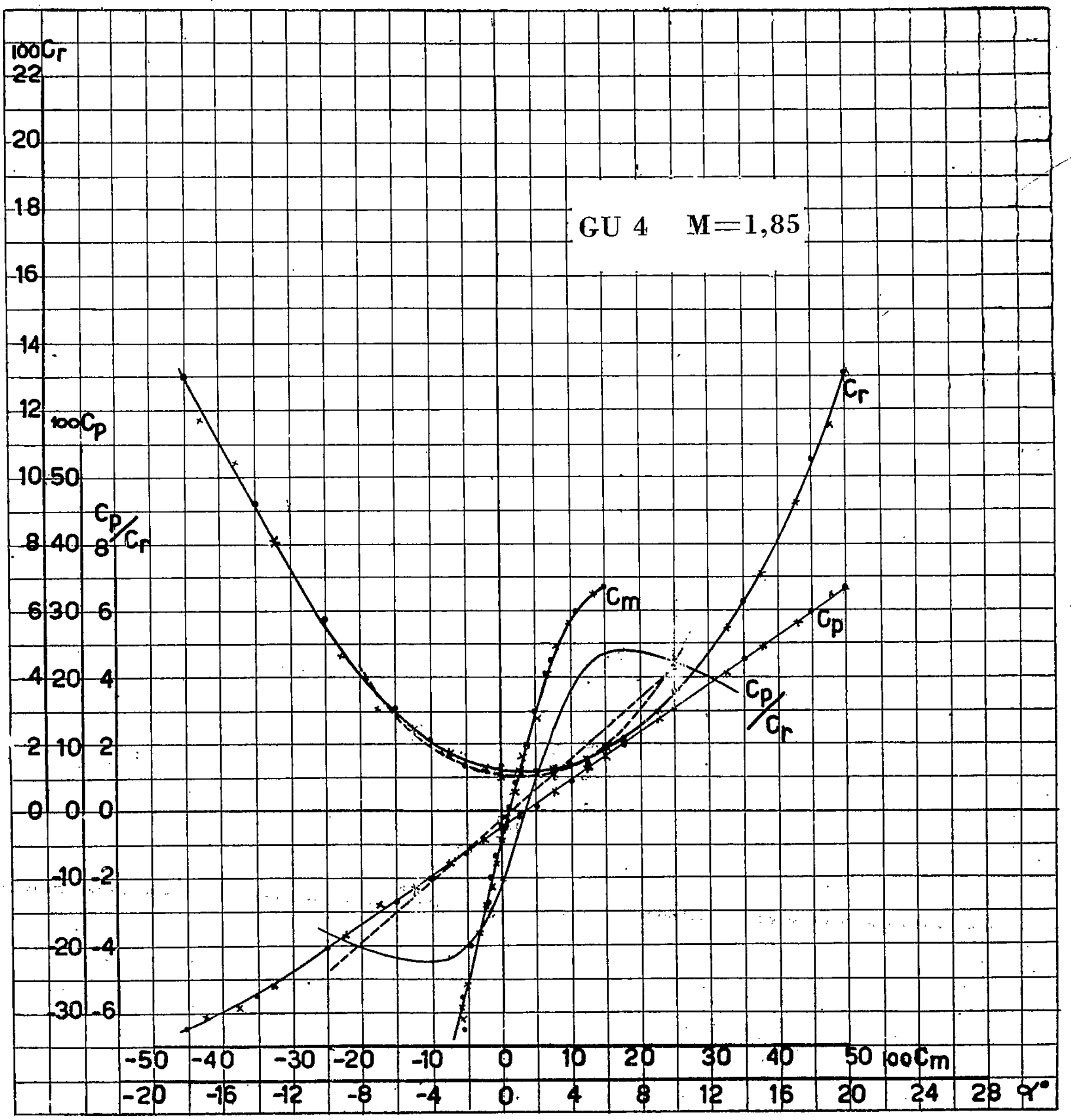

FIG. 8

α^0	-18^0	-16^0	-14^0	-12^0	-10^0	-8^0	-6^0
100 C_p	—31,4	—29,2 —29,7	—26,3	—23,5 —24,2	—20,1	—16 —15,8	—12,5 —13,2
100 C_r	13,81	11,95 11,80	9,49	6,85 7,38	5,55	4,15 4,15	2,95 3,15
100 C_m	—10,0	9,2 10,6	— 8,9	— 7,8 — 8,8	— 7,0	— 4,8 — 5,6	4,2 4,2

α^0	-4^0	-3^0	-2^0	-1^0	0^0	1^0	2^0
100 C_p	— 8,90 — 9,8	— 7,60	— 5,2 — 6,6	— 4,3	— 2,4 — 3,0	— 1,0	0,7 1,2
100 C_r	2,14 2,31	1,95	1,68 1,55	1,50	1,39 1,28	1,28	1,35 1,35
100 C_m	— 2,8 — 3,1	— 2,0	— 1,4 — 1,8	— 1,1	— 0,2 — 0.3	0,3	0,8 0,5

α^0	3^0	4^0	6^0	8^0	10^0	12^0	14^0
100 C_p	2,6	5,2 4,1	8,6 7,4	11,7 11,0	15,0	18,5 17,4	21,9
100 C_r	1,44	1,65 1,58	2,20 2,08	2,99 2,80	3,72	5,12 4,89	6,41
100 C_m	1,8	2,6 2,4	4,1 3,6	5,4 5,20	6,8	7,7 7,7	9,4

α^0	16^0	18^0	20^0
100 C_p	25,8 24,9	29,0	33,1
100 C_r	8,15 7,95	10,00	12,32
100 C_m	11,4 11,0	13,4	15,2

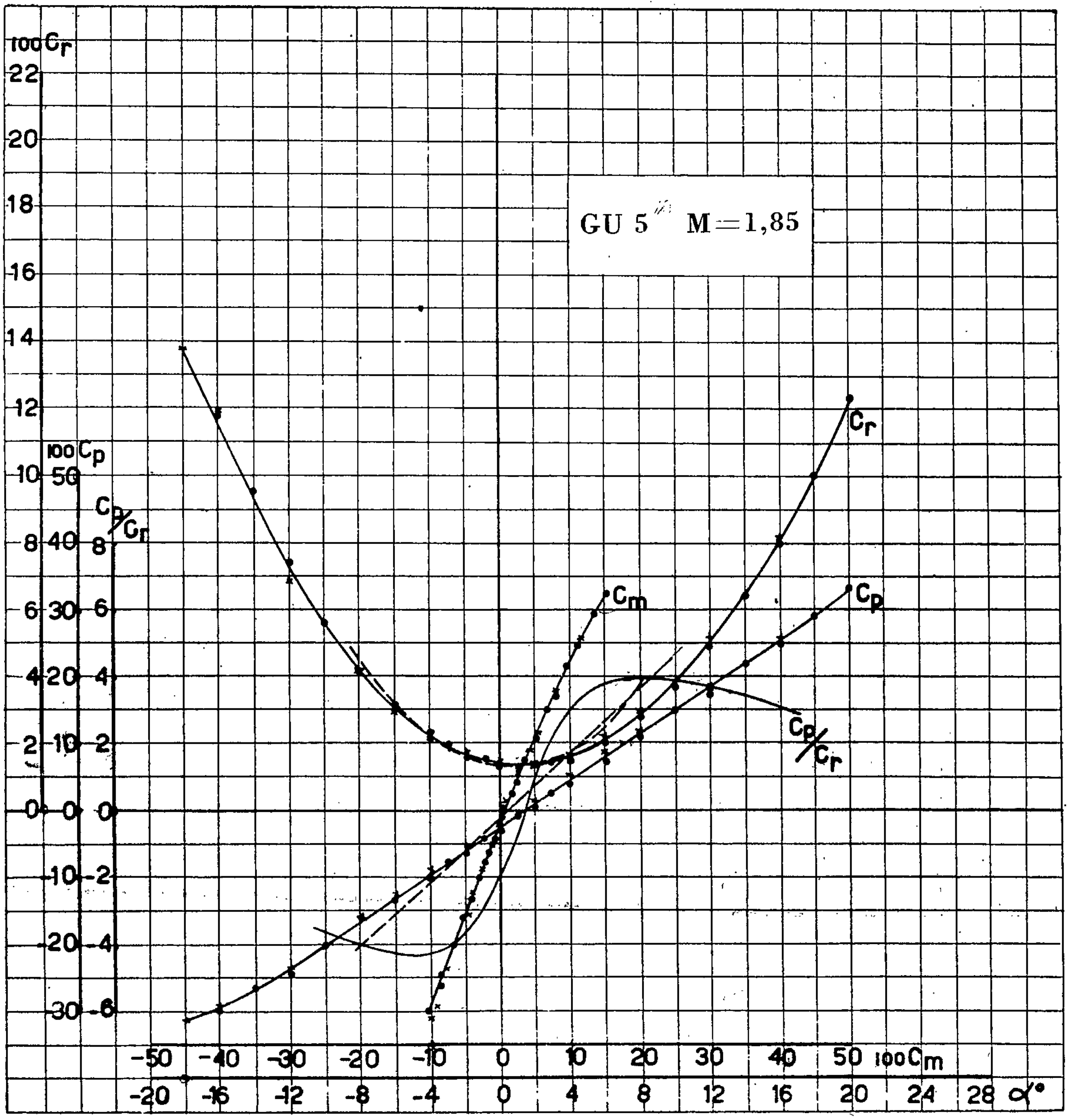

FIG. 9

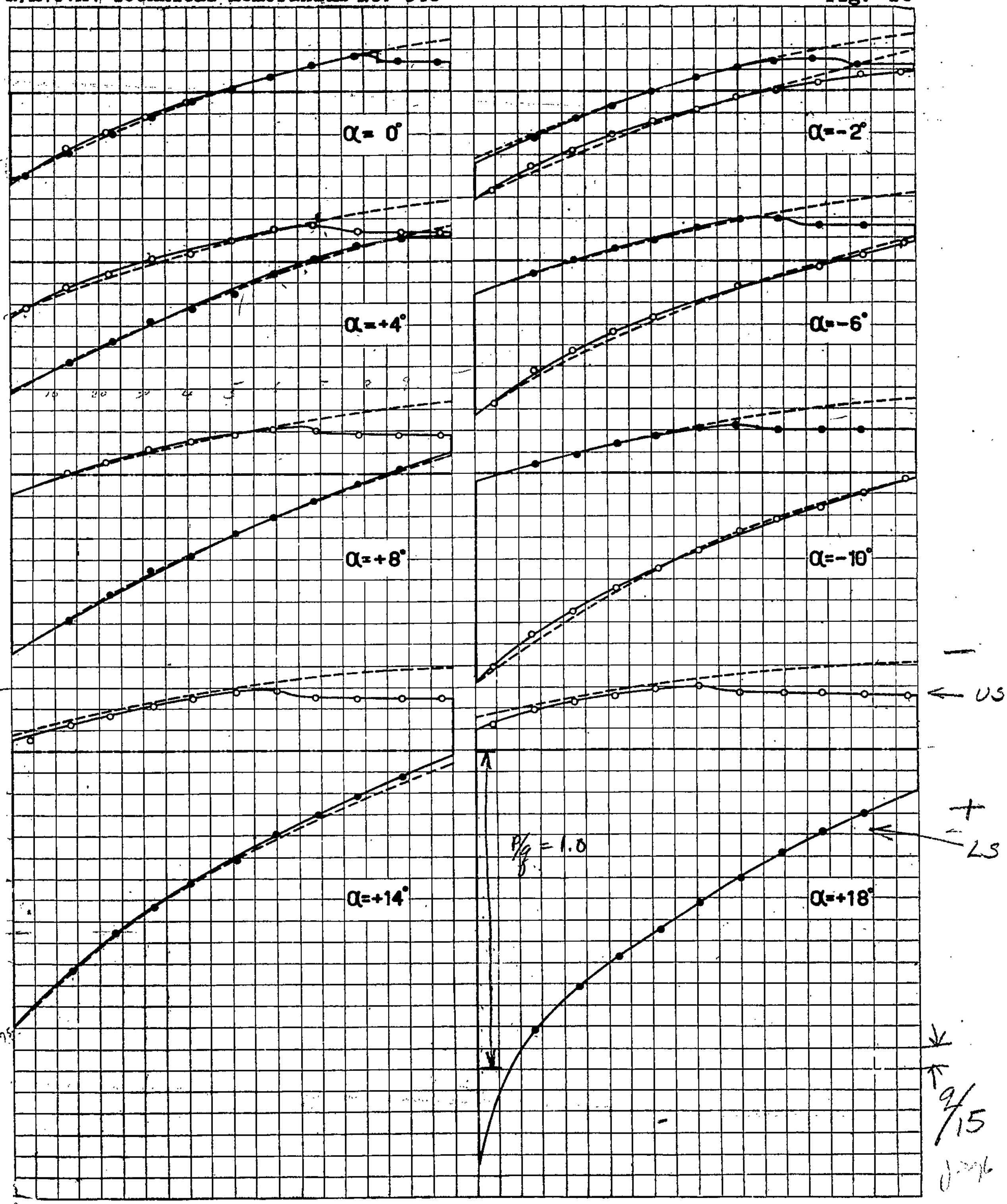

FIG. 10 (continued on following page)

GV-2
M- 2113

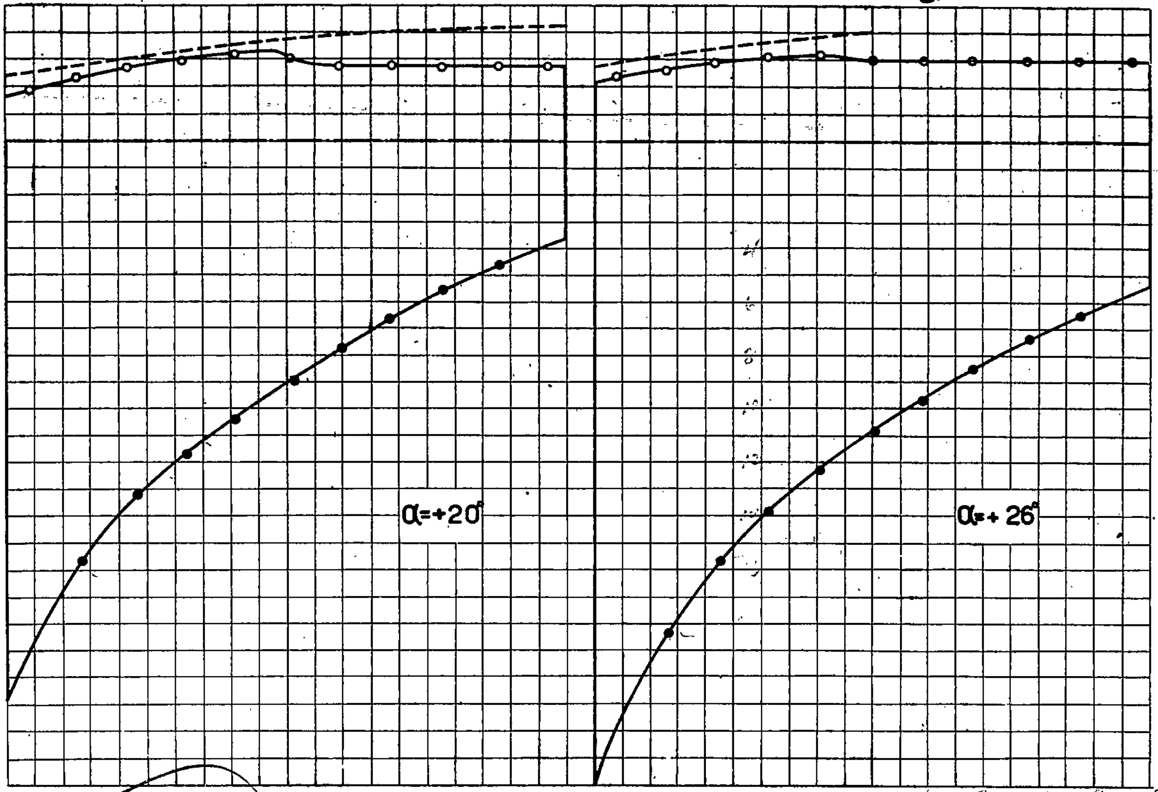

FIG. 10

GU 2 M = 2,13 R = 640000

Sta-tion	% Chord		α°	0	— 2	4	— 6	8	— 10	14	18	20	26
			p_o	52,1	52,2	52,3	52,3	52,2	52,2	52,2	52,2	52,2	52,5
			q	165,5	166	166,5	166,5	166,5	166	166	166	166	166
1	4	Top	$P_1 - P_0$	43	52	24,5	75	8	101	— 6	—13	—20	—26,5
2	12,5			29	39	13,5	58	— 1	85	—13,5	—20,5	—25	—29,5
3	21,5			20	37,5	5,5	47	— 6,5	72	—18	—25	—30	—32,5
4	31,0			12,5	22	— 2	37	—14	60	—23	—28	—33.5	—35
5	40,5			5	15	— 5,5	29	—18	50	—27	—32	—36	—37
6	50,5			— 1,5	11	—11	21	—21	41,5	—30	—33	—33,5	—34,5
7	59,0			— 7,5	3	—17	13	—24	30	—31,5	—30	—31	—33,5
8	68,5			—13,5	0	—20	7	—23	24,5	—27	—30	—31	—33,5
9	78,7			—18,5	— 4	—16,6	2	—21	17	—27	—29	—31	—33,5
10	87,5			—15,5	— 8,5	—16	— 4	—21	10	—27	—29	—31	—33,5
11	97,0			—15,5	—10	—16	—10	—21	2,5	—26	—28	—31	—33,5
12	13,6	Bottom		31	25	53	7	76	— 5	114,5	148	174	204
13	22,5			21	14,5	41,5	— 1	63	—10	95	124	148	174
14	31,5			13	8	31	— 7	50	—15	81	106,5	130	155
15	40,5			5	0	24,5	—11	43	—18,5	70	94	115	137
16	50,5			— 1,5	— 7	16	—17	31	—23,5	57,5	80	99	120
17	59,0			— 7,5	—12	5,5	—21	22 ~~32~~	—25	44	66	86	108
18	68,5			—14	—17	— 2,5	—22	14,5	—23	34	53	74	94
19	78,7			—18,5	—16,5	— 9	—19	5	—23	24	42,5	61	82
20	87,5			—15,5	—14	—13	—19	— 3	—23	13	34	51	71

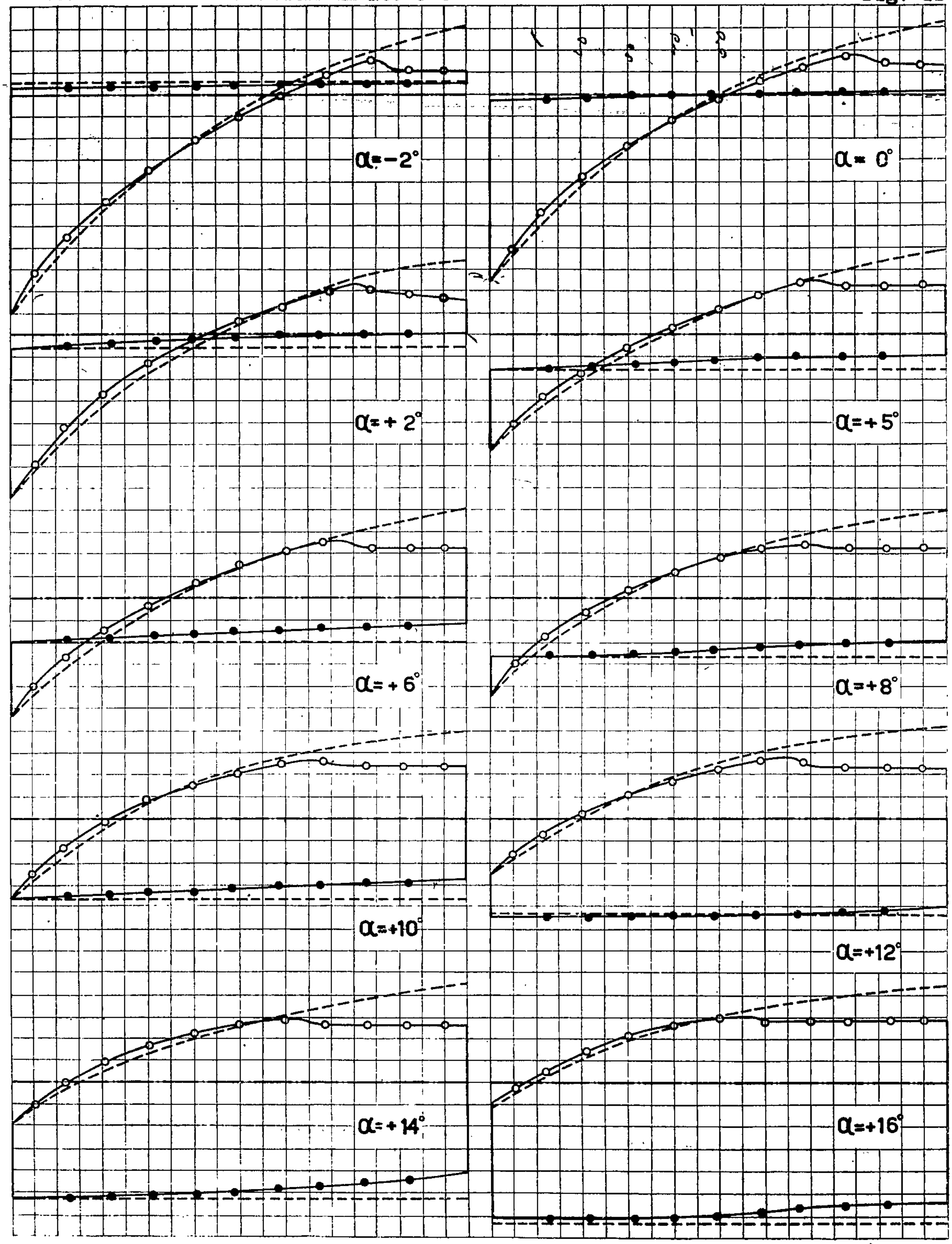

FIG. 11 (continued on following page)

GU 3
M = 2.13

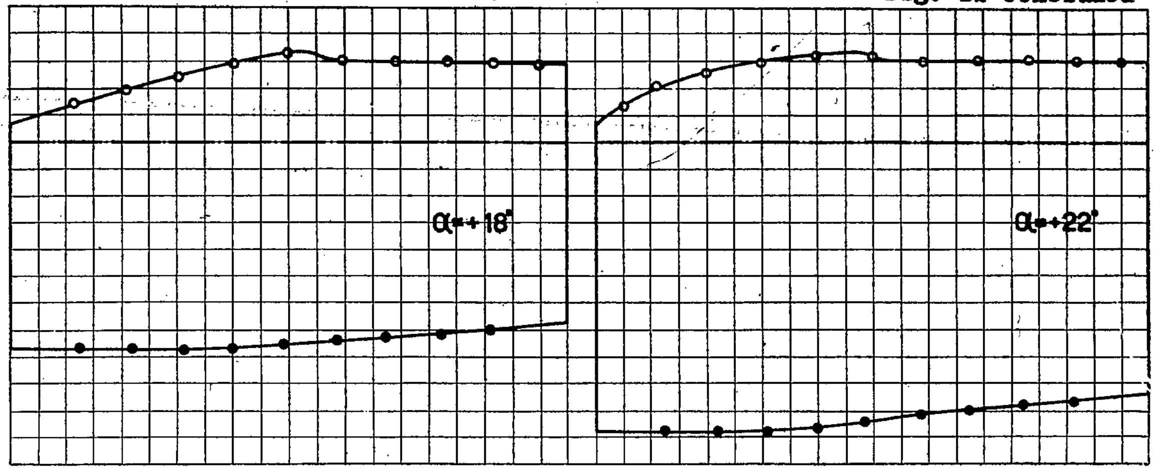

Fig. 11

GU 3 M = 2,13 $R = 710000$

Station	% Chord		−2	0	2	5	6	8	10	12	14	16	18	22
		α^0	−2	0	2	5	6	8	10	12	14	16	18	22
		p_o	57,4	57,4	57,4	57,4	57,4	57,4	57,4	57,4	57,4	57,4	57,4	57,4
		q	182,9	182,9	182,9	182,9	182,9	182,9	182,9	182,9	182,9	182,9	182,9	182,9
1	5	Top p_1 →	98,5	85	73	50	48,8	35,1	30,5	19,5	12,2	2,5	−12	−16
2	11,5	Top	79,1	65,8	52,4	34,1	33	22	22	8,5	0	−6,1	−17,2	−26
3	20,5	Top	60,2	45	34	20,7	17,2	8,5	1	−3,5	−12,1	−18	−24	−31
4	30	Top	41,1	28	17,1	7,3	4,3	−4,2	−11	−13,4	−19,5	−25,5	−29,5	−36
5	40	Top	24,4	14	3,67	−3,15	−8,5	−14,6	−19	−20,7	−27	−31	−36,5	−39
6	49	Top	12,2	2,4	−7	−14,6	−18,3	−22	−25	−26,8	−32	−36	−40	−39
7	59,2	Top	0	−7,3	−14,6	−22,5	−25,1	−27,1	−31	−34	−34	−34	−37	−36
8	68,4	Top	−11	−13,6	−23,3	−29,5	−30,5	−29,5	−32	−32	−32	−34	−37	−36,2
9	77,5	Top	−18,3	−21	−26	−25,2	−28	−28	−29,5	−29,2	−32	−34	−37	−36
10	86,2	Top	−13,4	−18,3	−22	−25,2	−28	−28	−29,5	−29,2	−32	−34	−37	−36
11	95	Top	−13,4	−18,3	−19,5	−25,2	−28	−28	−29,3	−29,2	−32	−34	−37	−36
12	12,5	Bottom	−4,2	2,4	7,3	19,5	23,3	31,8	42	55	63,2	75	94	131
13	22	Bottom	−4,8	2,2	5,5	18,7	22	31,1	41,5	55	63,1	75	93,5	131
14	31,5	Bottom	−4,8	1,8	3,6	16	20,7	30,5	39,5	55	63	75	94	130
15	40,5	Bottom	−4,8	1,2	3,1	15,1	19,5	29,9	39,5	53,4	62,1	75	93,2	129
16	50	Bottom	−4,8	0	2,4	14,6	18,4	28,7	39	53,4	60,5	74	91,5	128
17	58,6	Bottom	−5,5	0	1,2	12,8	17,6	26,8	36,5	53	58,7	71	90,3	123
18	67,6	Bottom	−5,5	−0,6	1,2	12,2	16,4	25,6	36	52,5	58	69	88,8	122
19	77,5	Bottom	−6,1	−1,2	0,7	12,2	15,2	24,4	34,7	51,1	55	68,3	86,5	119
20	86,2	Bottom	−6,1	−1,2	0	12,2	15	24,2	34,2	50	53,7	67	85,1	117,5

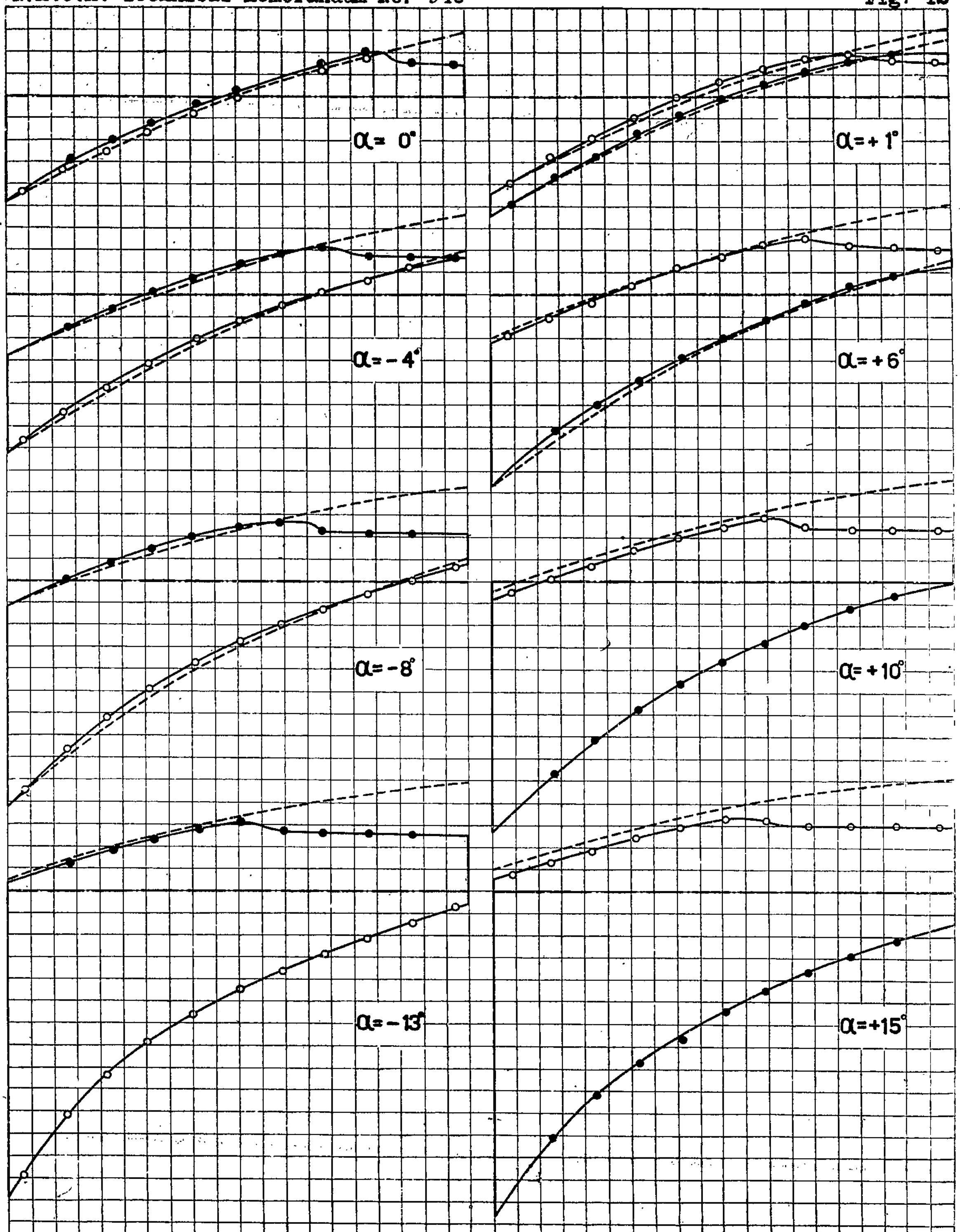

FIG. 12 (continued on following page)

GV-2
M=1.85

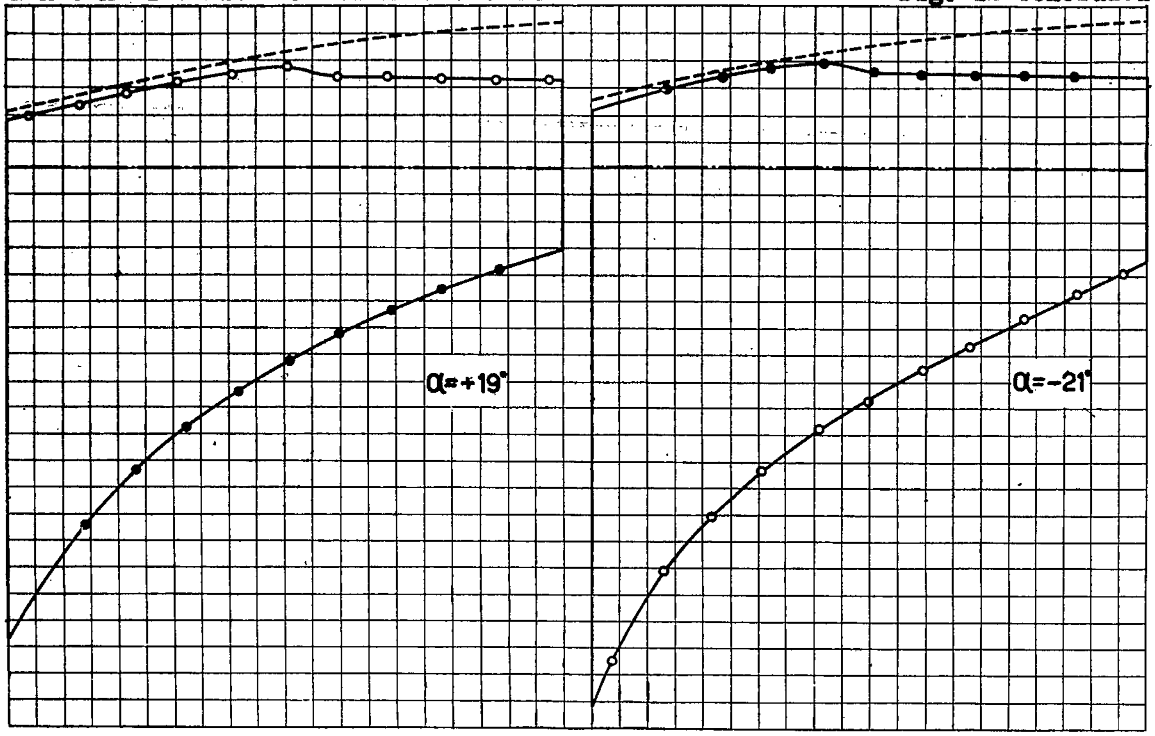

FIG. 12

GU 2 $M = 1,85$ $R = 720000$

Station	% Chord	α^0	0	1	− 4	6	− 8	10	− 13	15	+ 19	− 21
		p_s	80,5	80,5	80,5	80,5	80,5	80,5	80,5	80,5	80,5	80,5
		q	193,5	193,5	193,5	193,5	193,5	193,5	193,5	193,5	193,5	193,5
1	4	p_1	56	50	85	24	121	6	168	− 10	− 24	239
2	12,5		42	35	69	14	98	− 1,5	130	− 16,5	− 30	19 5
3	21,5		31	24	54	5	79	− 9	108	− 23	− 35	169
4	31		20	12	40	− 5	63	− 18	88	− 31	− 41	149
5	40,5	Top	8,5	1	25	− 15,5	47	− 26	72	− 37	− 44	129
6	50,5		− 1	− 8	15	− 22	34,5	− 31	57,5	− 42	− 48	113
7	59		− 10	− 16	6,5	− 28,5	24,5	− 37,5	47	− 41	− 43	98
8	68,5		− 16	− 22	− 1,5	− 33	16,5	− 32	37	− 39	− 43	86
9	78,7		− 23	− 25	− 8,5	− 28	7	− 31	27,5	− 38	− 42	72
10	87,5		− 20	− 21	− 16,5	− 27	− 1	− 31	18,5	− 37	− 42	60
11	97		− 18	− 20	− 22	− 26	− 9	− 30,5	9	− 37	− 42	50
12	13,5		37	47	18,5	79	− 1	112	− 16,5	143,5	174	− 37
13	22,5		25	35	8	65	− 11	94	− 23,5	118	146	− 43
14	31,5		15	21	− 2	50	− 19	74	− 30	99	126	− 48
15	40,5	Bottom	3,5	10	− 10	37	− 26	59	− 36,5	86	109	− 50
16	50,5		− 3	0	− 18,5	25	− 32,5	47	− 40	69	94	− 46
17	59		− 12	− 7	− 25	15	− 34,5	35	− 35	58	81	− 45
18	68,5		− 18	− 15	− 28,5	5	− 29	25	− 34	47	69	− 45
19	78,7		− 25,5	− 20	− 23	− 4,0	− 28	15	− 33	38	60	− 45
20	87,5		− 20	− 24,5	− 23	− 11	− 28	8	− 33	28	49	− 45

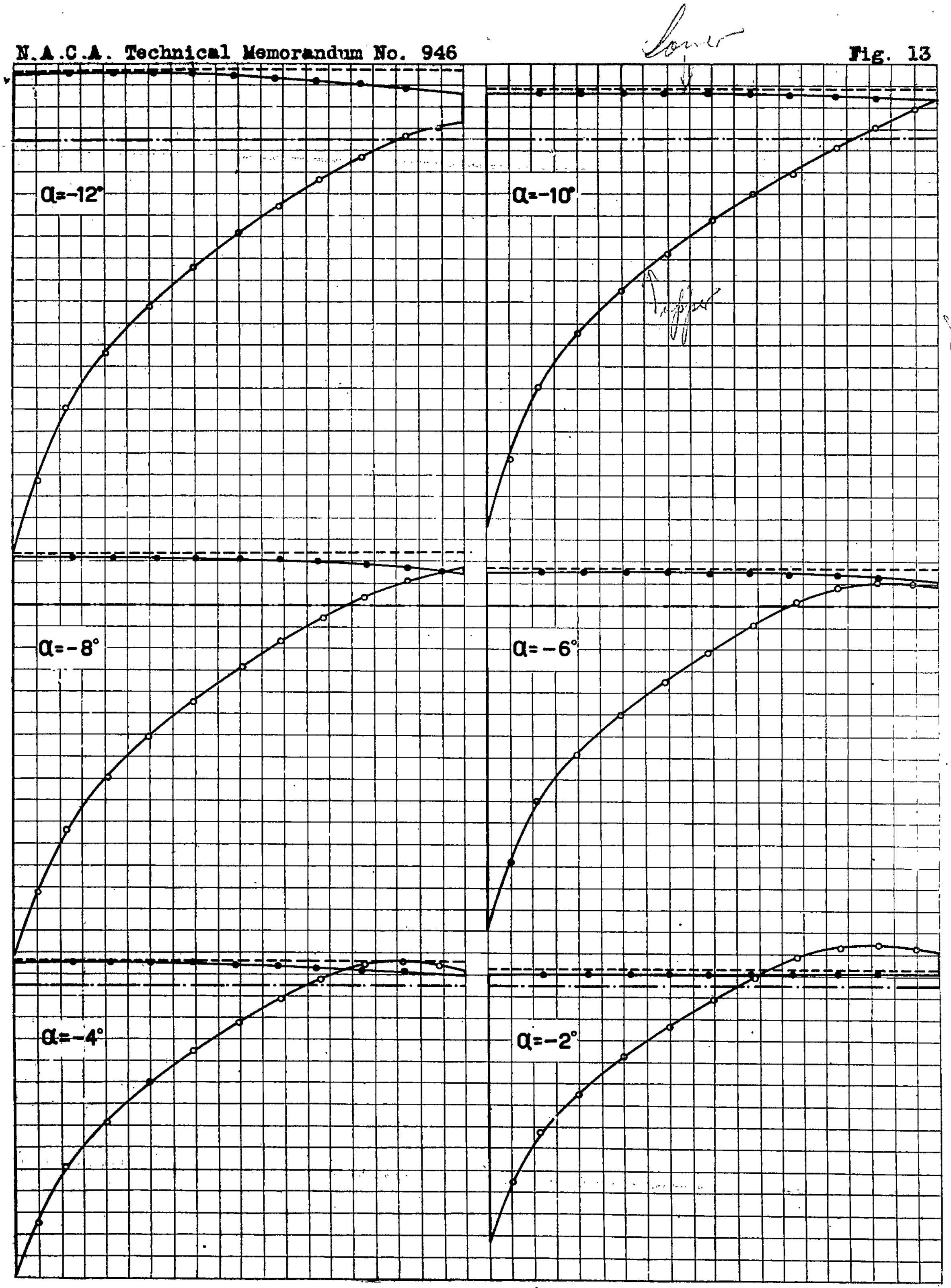

FIG. 13 (continued on following page)

GV-3
M = 1.85

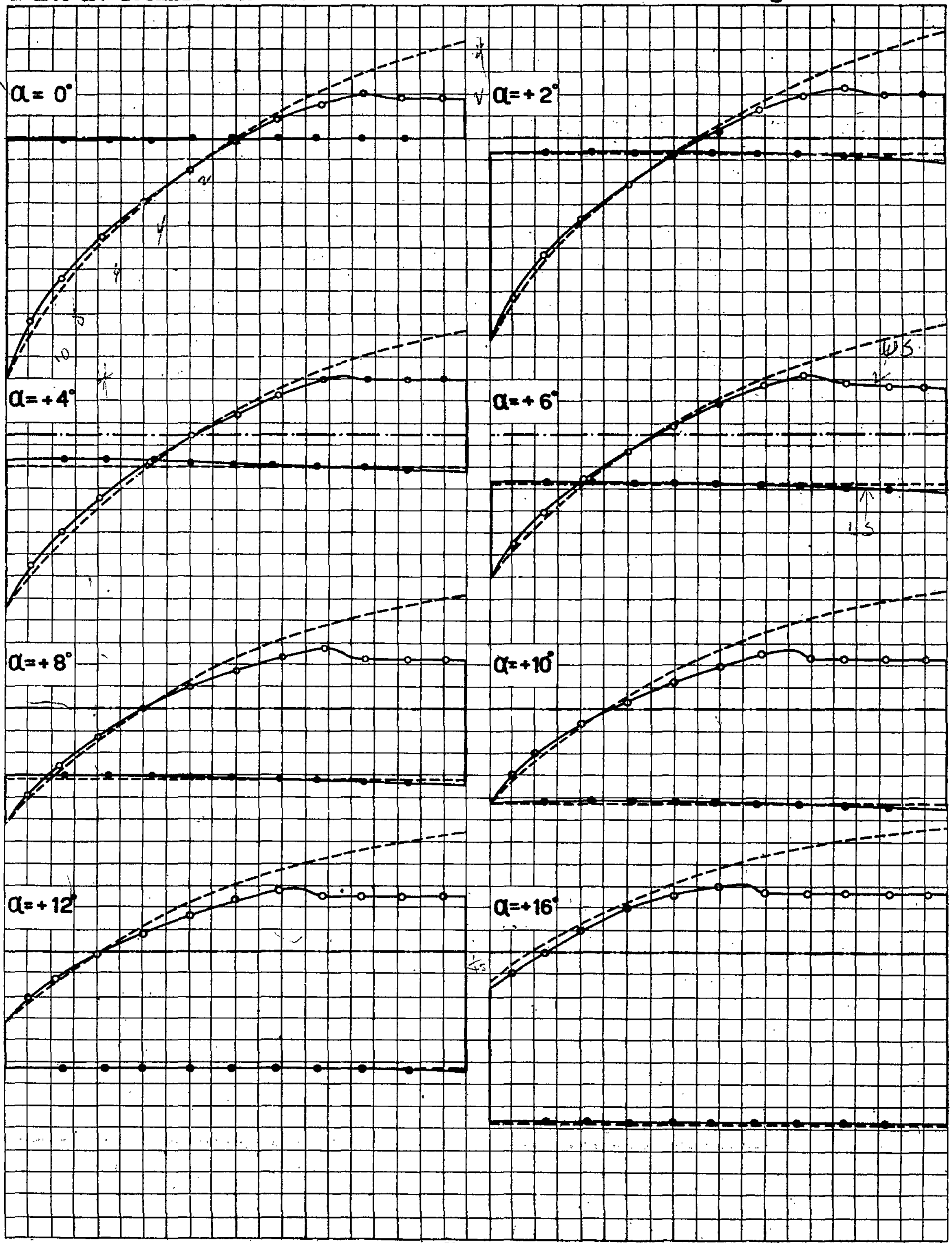

FIG. 13

GU 3
M = 1,85

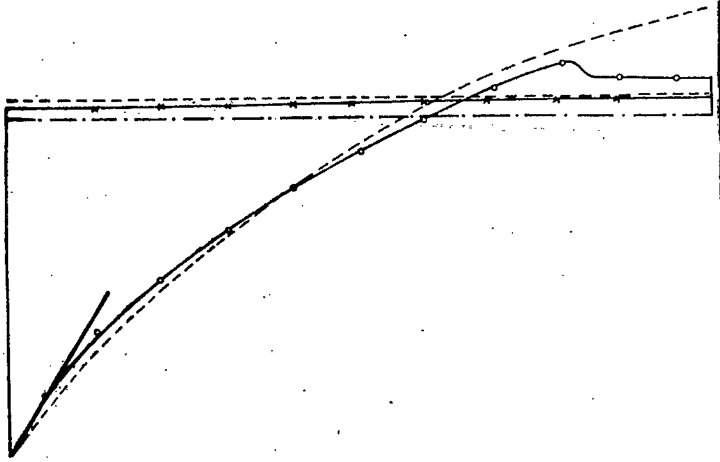

Figure 14.- Variation of the tangent to the pressure curve at the leading edge according to the theory of Crocco.

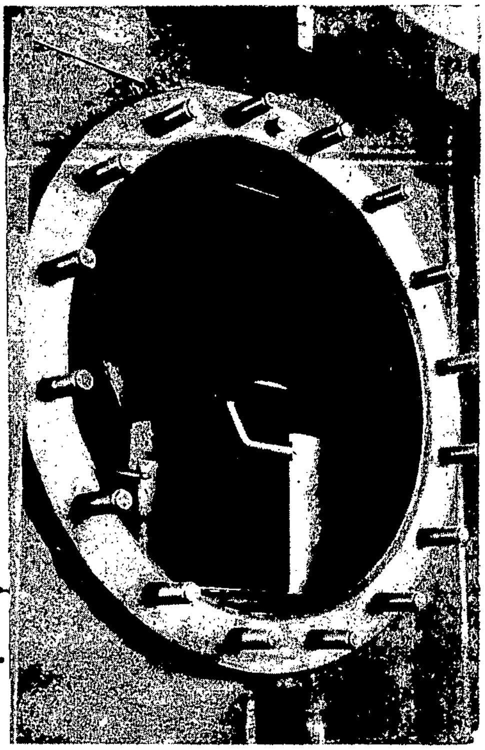

Figure 15.- Mounting of the model for photographic observations.

GU 3 M = 1,85 *R* = 730000

Station	% Chord															
		α^0	— 12	— 10	— 8	— 6	— 4	— 2	0	2	4	6	8	10	12	16
		p	80,05	80,05	80,05	80,05	80,05	80,05	80,02	80,05	80,05	80,05	80,05	80,05	80,05	80,05
		q	193,5	193,5	193,5	193,5	193,5	193,5	192,9	193,5	193,5	193.5	193,5	193,5	193,5	193,5
1	5	Top	204	191	173	152	140	116	106	94	76	65	52	39	28	11
2	11,5	Top	161	148,5	134	115	106	87	82,5	68	57,5	46	34	26	16	0
3	20,5	Top	128	115	103	88	80,5	65	58	48	37,5	27	17	8	— 2	— 14
4	30	Top	100	90	79	65	57	42,5	37	27	16	9	0	— 5	— 11	— 26
5	40	Top	77,5	69	58	45	38,5	26	18	10	0,5	— 4	— 11,5	— 15	— 20	— 33
6	49	Top	56	48.5	38	28	21	9	3	— 4	— 11	— 16	— 21	— 24,5	— 30	— 39
7	59,2	Top	41	33,5	22,5	11,5	6,5	— 4	— 11	— 15,5	— 23	— 28	— 28	— 32	— 36	— 33
8	68,4	Top	25,5	22	9,5	— 2	— 4	— 15,5	— 19,5	— 24,5	— 33	— 35	— 35	— 30	— 31,5	— 33
9	77,5	Top	12,5	5,5	— 2,5	— 10	— 13	— 22	— 26	— 30	— 31,5	— 29	— 27	— 30	— 31.5	— 33
10	86,2	Top	0	— 6,5	— 12	— 14	— 14,5	— 24	— 23	— 24,5	— 31,5	— 28	— 27	— 29	— 31,5	— 33
11	95	Top	— 5,5	— 17	— 17,5	— 12	— 12	— 21	— 23	— 24,5	— 31,5	— 27,5	— 27	— 29	— 31,5	— 33
12	12,5	Bottom	— 39	— 27	— 27	— 20,5	— 15	— 7	1	8	14,5	28	39	51	68	99
13	22	Bottom	— 39	— 27	— 27	— 20,5	— 15	— 7	1	8	15	28	39	51	68	99
14	31,5	Bottom	— 39	— 27	— 26,5	— 20,5	— 15	— 6,5	1	8	15	29	40	51	68	98
15	40,5	Bottom	— 38,5	— 27	— 26	— 20,5	— 14	— 6,5	0	8,5	16,5	30	40	52	68	99
16	50	Bottom	— 37	— 26,5	— 25,5	— 19,5	— 13	— 6,5	0	8,5	17	29	40	52	68	98
17	58,6	Bottom	— 35	— 26	— 24,5	— 19,5	— 11,5	— 6,5	0	9	17,5	30	41	53	68,5	99
18	67,6	Bottom	— 33,5	— 25	— 24	— 19	— 11	— 6	0	9,5	18,5	31	42	54	69	100
19	77,5	Bottom	— 31	— 24,5	— 21,5	— 18	— 9,5	— 5,5	1	10	19	33	43	56	70	99
20	86.2	Bottom	— 28,5	— 23	— 20	— 16	— 8,5	— 5,5	0	10,3	20,5	33	44	56	70	99

Fig. 16 - Prof. G. U. 6 M = 1,85 α = —12°

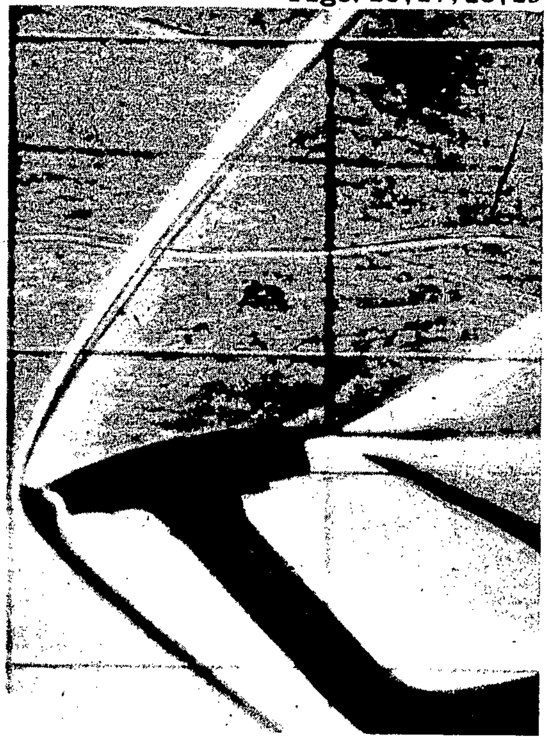

Fig. 17 - Prof. G. M. 6 M = 1,85 α = —12°

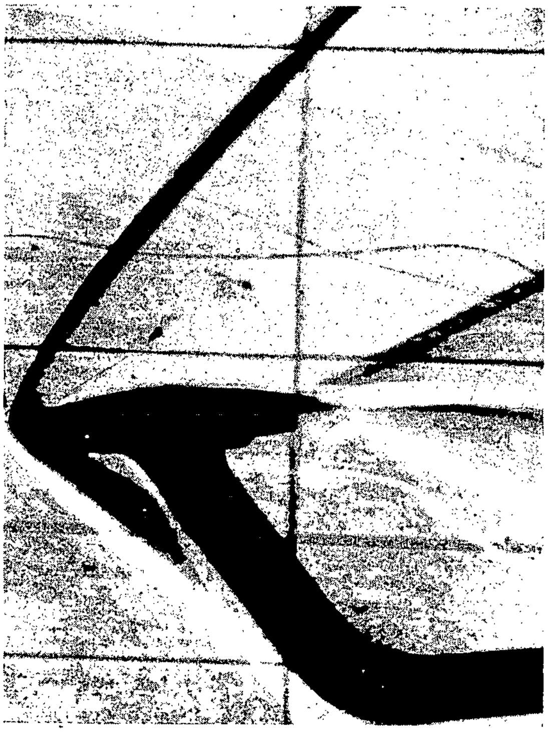

Fig. 18 - Prof. G. U. 6 M = 1,85 α = — 8°

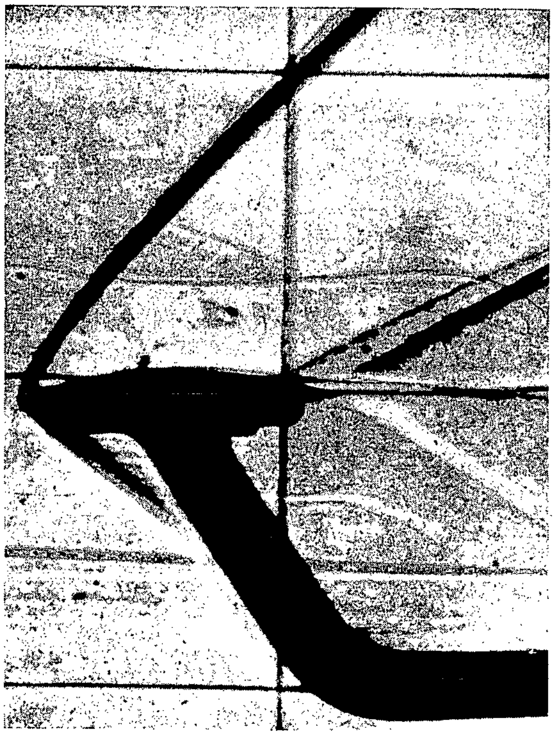

Fig. 19 - Prof. G. U. 6 M = 1,85 α = — 4°

Fig. 20 - Prof. G. U. 6 M=1,85 $\alpha=-2°$

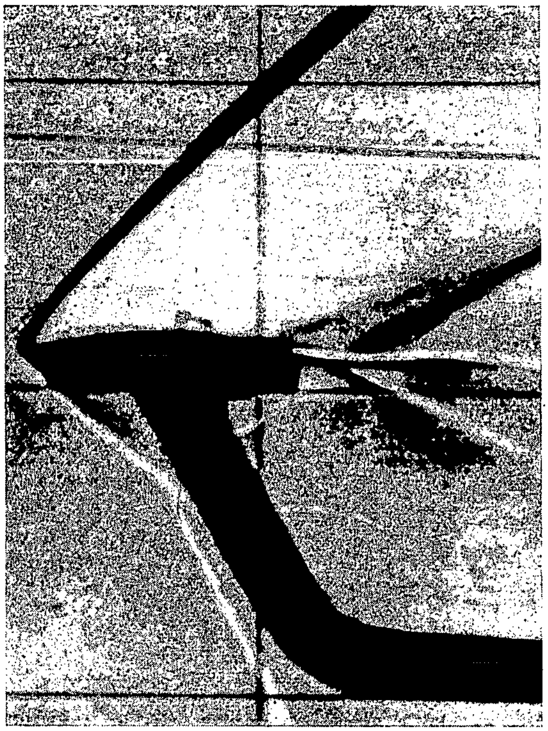

Fig. 21 - Prof. G. U. 6 M=1,85 $\alpha=0°$

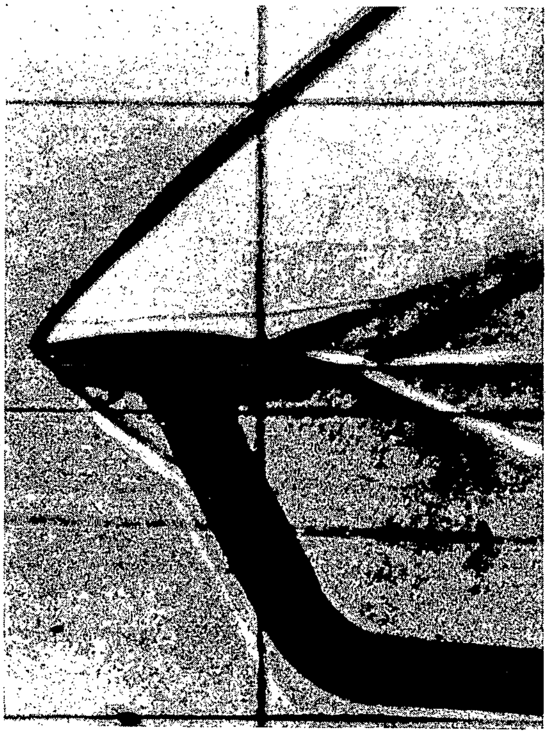

Fig. 22 - Prof. G. U. 6 M=1,85 $\alpha=2°$

Fig. 23 - Prof. G. U. 6 M=1,85 $\alpha=4°$

Fig. 24 - Prof. G. U. 6 M=1,85 α=8°

Fig. 25 - Prof. G. U. 6 M=1,85 α=8°

Fig. 26 - Prof. G. U. 6 M=1,85 α=12°

Fig. 27 - Prof. G. U. 6 M=1,85 α=12°

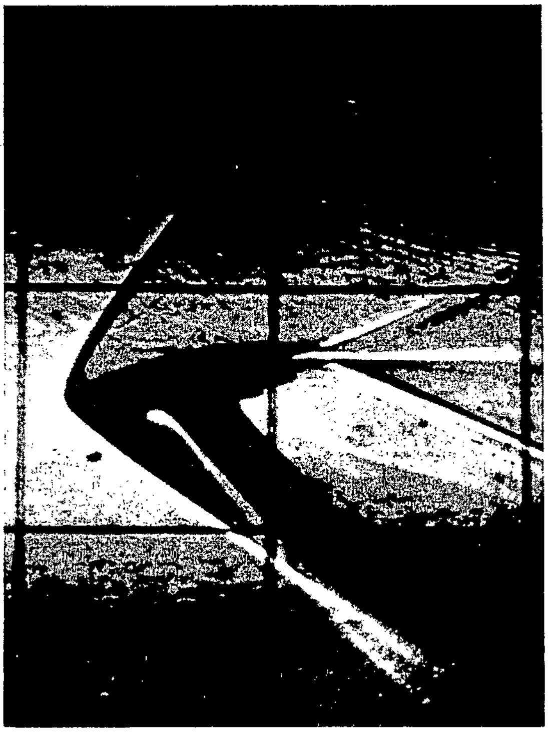

FIG. 28 - PROF. G. U. 6 M=2,13 $\alpha=-12°$

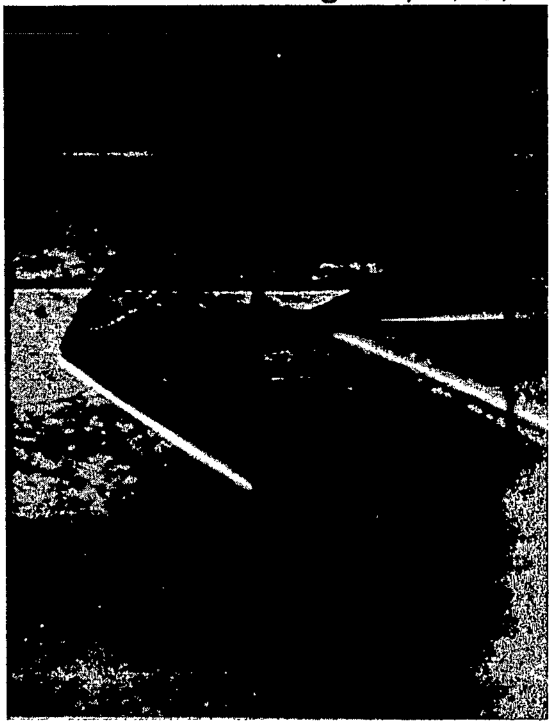

FIG. 29 - PROF. G. U. 6 M=2,13 $\alpha=-8°$

FIG. 30 - PROF. G. U. 6 M=2,13 $\alpha=-4°$

FIG. 31 - PROF. G. U. 6 M=2,13 $\alpha=-2°$

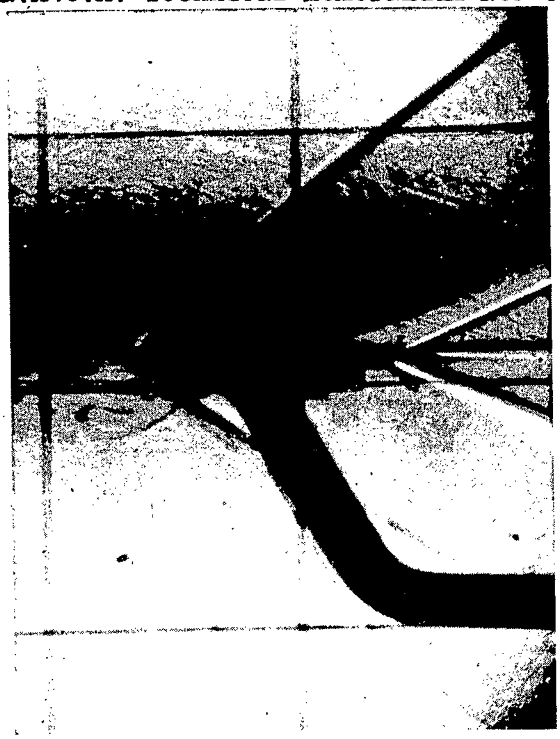

FIG. 32 - PROF. G. U. 6 M=2,13 $\alpha=0°$

FIG. 33 - PROF. G. U. 6 M=2,13 $\alpha=2°$

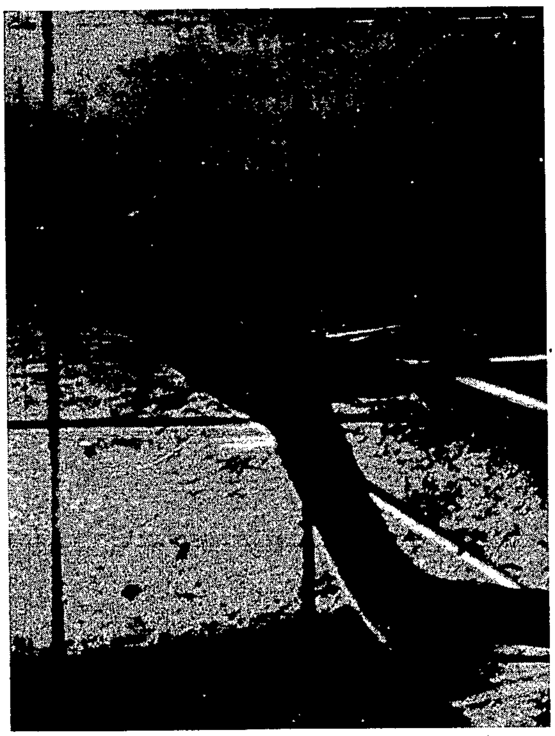

FIG. 34 - PROF. G. U. 6 M=2,13 $\alpha=4°$

FIG. 35 - PROF. G. U. 6 M=2,13 $\alpha=8°$

FIG. 36 - PROF. G. U. 7 M = 2,13 $\alpha = 0°$

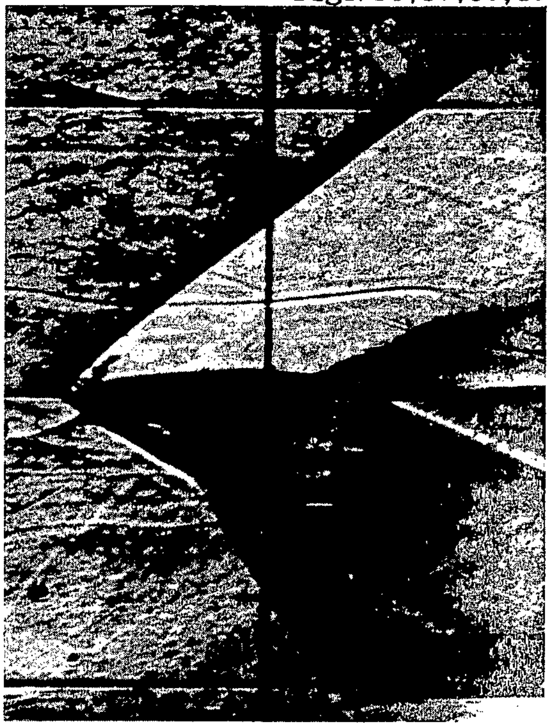

FIG. 37 - PROF. G. U. 7 M = 2,13 $\alpha = -2°$

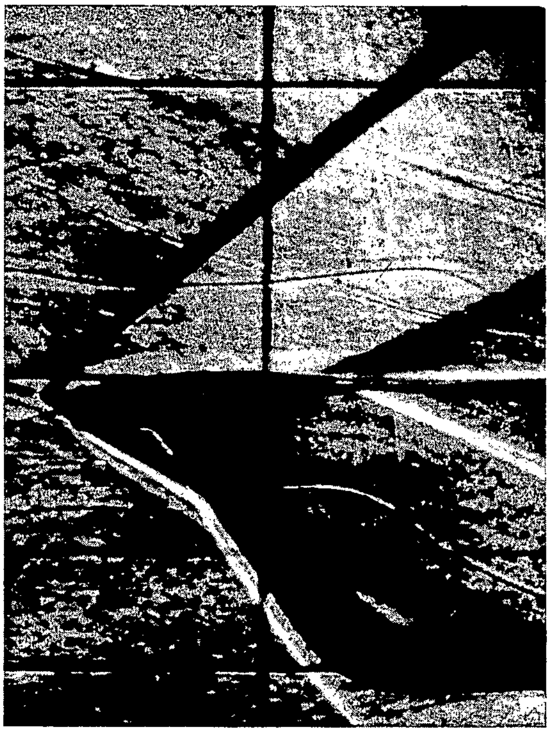

FIG. 38 - PROF. G. U. 7 M = 2,13 $\alpha = -4°$

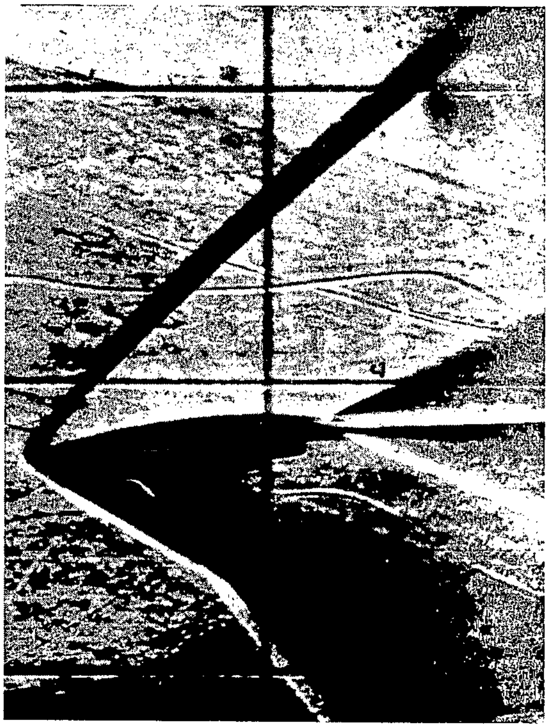

FIG. 39 - PROF. G. U. 7 M = 2,13 $\alpha = -8°$

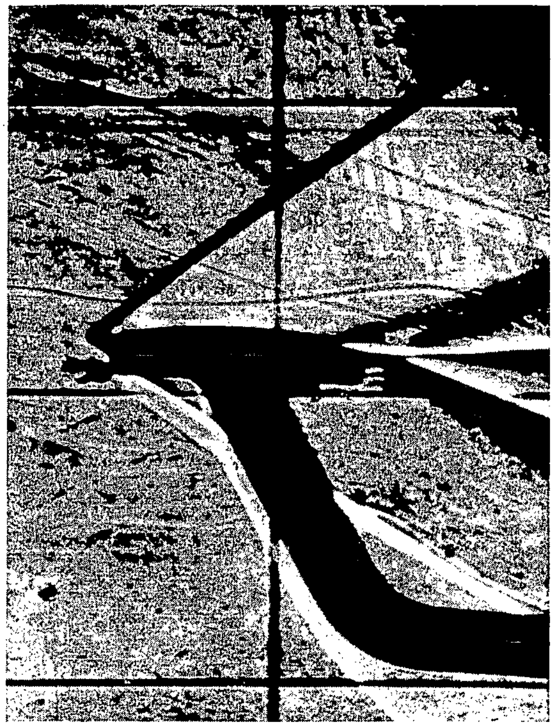

FIG. 40 - PROF. G. U. 7 M=2,13 $\alpha=2°$

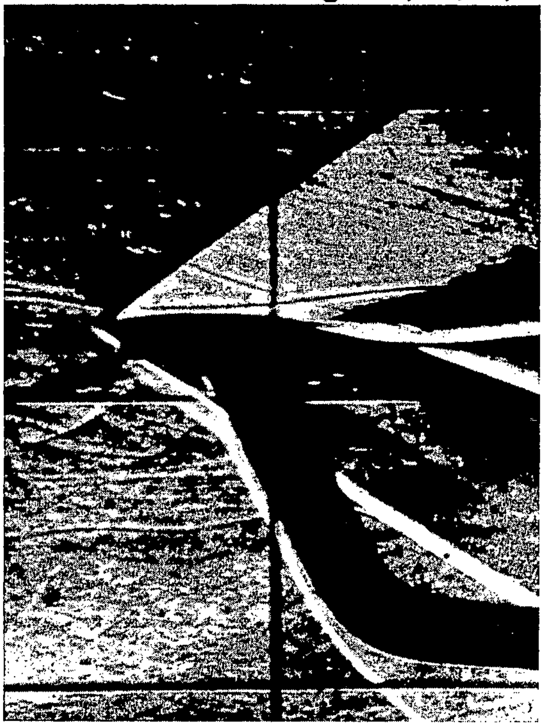

FIG. 41 - PROF. G. U. 7 M=2,13 $\alpha=4°$

FIG. 42 - PROF. G. U. 7 M=2,13 $\alpha=8°$

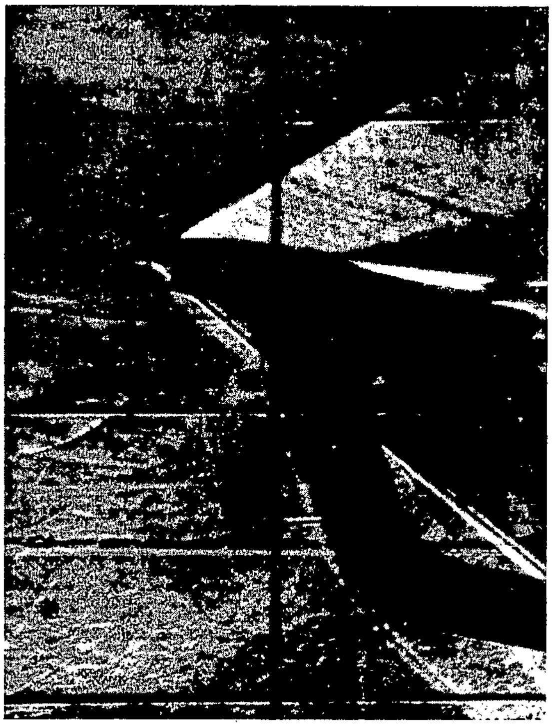

FIG. 43 - PROF. G. U. 7 M=2,13 $\alpha=12°$

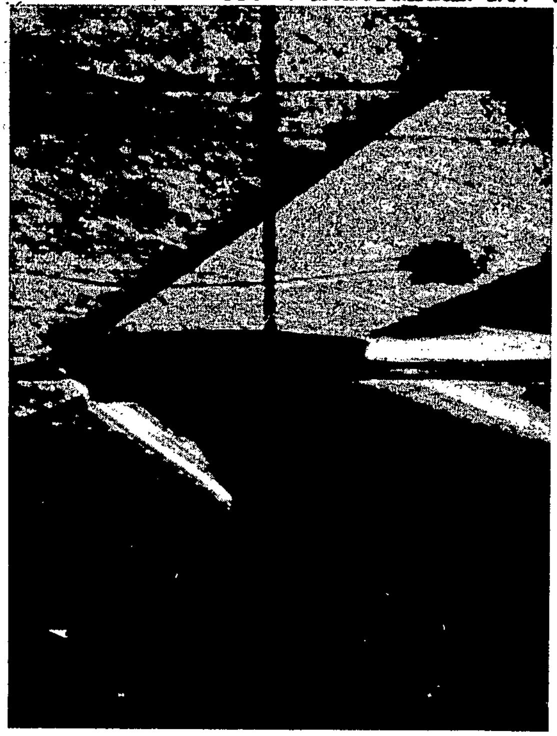

FIG. 44 - PROF. G. U. 8 M = 2,13 $\alpha = -2°$

FIG. 45 - PROF. G. U. 8 M = 2,13 $\alpha = 4°$

FIG. 46 - PROF. G. U. 8 M = 2,13 $\alpha = 8°$

FIG. 47 - PROF. G. U. 8 M = 2,13 $\alpha = 12°$